

Partially implicit Runge-Kutta methods for wave-like equations

I. Cordero-Carrión^a, P. Cerdá-Durán^b

^a*Departamento de Matemáticas, University of Valencia, C/ Dr. Moliner, 50, E-46100 Burjassot, Spain*

^b*Departamento de Astronomía y Astrofísica, University of Valencia, C/ Dr. Moliner, 50, E-46100 Burjassot, Spain*

Abstract

In this work we present a new class of Runge-Kutta (RK) methods for solving systems of hyperbolic equations with a particular structure, generalization of a wave-equation. The new methods are *partially implicit* in the sense that a proper subset of the equations of the system contains some terms which are treated implicitly. These methods can be viewed as a particular case of the implicit-explicit (IMEX) RK methods for systems of equations with wave-like structure. For these systems, the optimal methods with the new structure are easier to derive than the IMEX ones, specially when aiming at higher-order (up to fourth-order in this work). The methods are constructed considering the classical strong-stability-preserving optimal explicit RK methods for the purely explicit part. The resulting partially implicit RK methods do not require any inversion of operators and hence their computational cost per iteration is similar to those of explicit RK methods. We analyse the stability and convergence properties and show their practical applicability in several numerical examples. Our results show that, compared with explicit RK methods, the new methods have better stability properties (larger steps are allowed) and in general show smaller discretization error.

Keywords: ODEs; Runge-Kutta methods; IMEX; wave equation.

1. Introduction

The evolution in time of many complex systems, governed by partial differential equations (PDE), implies, in a broad variety of cases, looking for the numerical solution of a system of ordinary differential equations (ODEs). The most commonly used methods to integrate in time these systems of ODEs are the well-known Runge-Kutta (RK) schemes (see e.g. [1] for a general review of these methods and their main properties). Several classifications of the RK methods can be done, according to, e.g., their convergence order, the number of stages or their explicit/implicit structure. The numerical stability of different numerical methods depends on the particular structure of the equations being solved. Therefore, it is necessary to choose the appropriate numerical scheme tailored to the particular necessities of the problem being solved.

The presence of stiff terms in systems of PDEs can lead to numerical instabilities if explicit RK (ERK, hereafter) schemes are used. A possible solution is the use of an implicit or partially implicit method in order to have numerically stable solutions without large constraints in the step size of the discretisation. As an example, the (implicit) backward Euler method is numerically stable in cases where the (explicit) forward Euler method would fail (see e.g. [1]). As a second example, the so-called implicit-explicit (IMEX) RK methods have been used to solve convection-diffusion-reaction equations [2, 3, 4, 5], in situations where explicit methods would have failed. However, there are problems which, despite of not being stiff, still could benefit of the implicit character of a numerical method. In this work we refer to stiff problems as those in which there is a large separation of scales. In these kind of problems explicit methods fail when the step size is adapted to the slowest varying scale but not to the fastest one (see examples in [8]). However, in a more general sense stiffness can be defined as those cases in which explicit methods fail [10]. With the latter definition, the previous example could be called stiff. Further discussion about the different definitions of stiffness can be found in e.g. [9].

Let us consider, as an example, the harmonic oscillator

$$u_{tt} + \omega^2 u = 0, \tag{1}$$

ω being a real constant. If we define $v \equiv u_t$, this equation can be written as a system of first-order ODEs. In matrix form the system reads:

$$U_t = AU \quad ; \quad U \equiv \begin{pmatrix} u \\ v \end{pmatrix} \quad ; \quad A \equiv \begin{pmatrix} 0 & 1 \\ -\omega^2 & 0 \end{pmatrix}. \quad (2)$$

Let us consider three different first-order integration methods:

$$U_n = U_{n-1} + hAU_{n-1}, \quad (\text{Euler method}) \quad (3)$$

$$U_n = U_{n-1} + hAU_n, \quad (\text{implicit Euler method}) \quad (4)$$

$$U_n = U_{n-1} + h \begin{pmatrix} 0 & 1 \\ 0 & 0 \end{pmatrix} U_{n-1} + h \begin{pmatrix} 0 & 0 \\ -\omega^2 & 0 \end{pmatrix} U_n, \quad (\text{semi-implicit Euler method}) \quad (5)$$

being h a fixed step size. Note that the semi-implicit Euler method is also known as symplectic Euler [6] due to its symplectic properties. A necessary condition for the stability of the method (A-stability, see e.g. [1]) is that the eigenvalues of the iteration matrix, e , are such that $|e| \leq 1$. For the three methods described above these are given by (see e.g. [7], Sect. I.5.2):

$$e = 1 + h\sigma, \quad (\text{Euler method}) \quad (6)$$

$$e = (1 - h\sigma)^{-1}, \quad (\text{implicit Euler method}) \quad (7)$$

$$e^2 - (2 + h^2\sigma^2)e + 1 = 0, \quad (\text{semi-implicit Euler method}) \quad (8)$$

being σ the eigenvalues of the matrix A , which in this example are $\sigma = \pm i\omega$. As a result, the explicit Euler method is unstable for any value of $h > 0$, while the implicit Euler method does not suffer from this instability for any $h \geq 0$. The semi-implicit Euler is stable for $|h\omega| < 2$. This simple system is a clear example of a case in which, despite of not being stiff, an explicit method fails, while an implicit or semi-implicit method solves this numerical instability problem, at least for reasonable values of h . It seems natural to question whether we can identify a class of non-stiff problems which suffer from numerical instabilities if solved using explicit methods, and whether this instabilities can be cured by adding some implicit treatment in the numerical method.

In this work we focus on systems of ODEs describing oscillatory behaviour or, in the case of PDEs, describing wave-like behaviour. A proper definition is given in the next section. Although this class of systems is not completely general, it is relevant for a large class of problems in many fields of mathematics, physics and engineering. Examples of applications in which it is necessary to solve systems of ODEs resulting in highly oscillatory solutions are: calculation of periodic orbits (see e.g. discussion in [7]); dynamics of biological systems, e.g. Lotka-Volterra equations for the modelling of predator-prey systems (see e.g. [1]); electromagnetic transients in circuit networks (see e.g. [11]); molecular dynamics simulations (see e.g. [12]) and computer animation (see e.g. [14]), among others. Examples of applications in which it is necessary to solve wave equations for either scalar or tensional variables are: Klein-Gordon equations, with applications in solid state physics, nonlinear optics and quantum field theory; Maxwell equations, with applications in antenna design, medical imaging, photonics and geophysics (ground penetrating radar), e.g. FDTD methods [13]; Einstein equations describing gravitational radiation, with applications in gravitational wave astronomy; Navier-Cauchy equations for linear elasticity, with applications in seismology, among others. Additionally, in fluid dynamics one can find multiple cases of systems of equations which admit solutions in form of waves and hence fall into the class of systems under study. Examples of such systems are the Navier-Stokes equations for compressible fluids and shallow water equations, with interest in oceanography, among others.

In most of the cases above, examples in the literature can be found where explicit method show unstable behaviour or limit in excess the step-size. In those cases the customary solution is using a numerical method with some degree of implicitness. For systems of ODEs the semi-implicit (symplectic) Euler method is known to have better stability properties than the explicit Euler one for many of the examples above (see discussion on orbits and Lotka-Volterra equations in [1, 7] and an example for electromagnetic transients in [16]). For

cases involving the integration of trajectories (orbits, molecular dynamics, computer animation) the Verlet algorithm (also its variant velocity-Verlet) and leapfrog method are commonly used. Note that all these methods (semi-implicit Euler, Verlet, leapfrog) are very similar in their construction, they have symplectic properties and they are stable for systems with imaginary eigenvalues (as in the case of oscillatory systems). One important feature of these methods is that they are applicable to systems of ODEs in which one of the variables is updated first and the updated value is used to update the second variable. So despite of being explicit methods, they contain some degree of implicitness. We refer to methods sharing the latter property as *partially implicit*, which we will define more precisely in the next sections. Some of these instability problems are partially solved when using higher-order explicit Runge-Kutta (RK) schemes (as the popular fourth-order RK, see [15] for their stability properties). Alternatively explicit (e.g. Adams-Bashford) or implicit (Adams-Moulton) linear multi-step methods improve the stability properties, albeit at the expense in increasing the complexity of the algorithm [1]. For systems with a Hamiltonian description (e.g. orbits) higher-order symplectic methods have been used traditionally to ensure stability and high accuracy (see e.g. [7]). For wave-like equations it is also possible to find cases where an improvement over the explicit Euler method has been reported when adding some degree of implicitness: the FDTD method to solve Maxwell equations uses a staggered method (partially implicit in our notation) to prevent numerical instabilities [13]. There have been attempts to improve the stability of the original FDTD method using the semi-implicit Euler method [17] or fully implicit ones [18]. Similarly, [19] proposed a staggered method, similar to FDTD, to solve Schrödinger equations. In the case of Einstein equations the numerical instabilities in the first simulations of black hole mergers were overcome by a variant of the Verlet method [20] or using the partially implicit Crank-Nicholson method (see e.g. [21]); nowadays, the most popular time integrators for the Einstein equations are explicit high-order Runge-Kutta methods (fourth or higher-order, see [22]), although some amount of Kreiss-Olinger numerical dissipation [23] is usually necessary to have numerical stability [22].

The goal of this work is to derive a set of numerical methods which are an extension of the semi-implicit Euler method to higher-orders in the sense that they are partially implicit (but without its symplectic behaviour). We present partially implicit RK (PIRK) methods of up to fourth-order which are applicable to wave-like equations. These new PIRK methods can be viewed as a particular case of the IMEX RK methods applied to systems of equations with a particular structure (wave-like), but their derivation, as shown in this paper, is much simpler, allowing us to derive relatively easy methods up to fourth-order of convergence. The PIRK methods are able to provide stable evolutions due to their implicit component, but they do not require any analytical or numerical inversion of operators, so their computational costs are similar to those of the ERK methods. This provides a great advantage with respect to implicit or IMEX methods which need, in general, an inversion of some operators; depending on the complexity of the equations, the inversion can be done analytically or numerically, or be even prohibitive in practice from the numerical point of view. The choice of the coefficients in their derivation are based on stability properties for both the explicit and implicit parts, as it is described in the following sections. The methods are validated by several numerical examples, for which stable evolutions are obtained, and compared with the results obtained by using ERK methods.

The manuscript is organized as follows. In Sect. 2 we introduce the definition of *system of wave-like equations*. The structure of the PIRK methods, applied to this kind of equations is described in Sect. 3. In Sect. 4 we derive the PIRK methods up to fourth-order by analysing their stability properties. In Sects. 5 to 7 we present numerical applications of the PIRK methods showing their stability and convergence properties. Conclusions are drawn in Sect. 8.

2. Systems of wave-like equations

Let us consider the following system of PDEs,

$$\begin{cases} u_t = \mathcal{L}_1(u, v), \\ v_t = \mathcal{L}_2(u) + \mathcal{L}_3(u, v), \end{cases} \quad (9)$$

being \mathcal{L}_1 , \mathcal{L}_2 and \mathcal{L}_3 general non-linear differential operators. Note that \mathcal{L}_1 and \mathcal{L}_3 depend on both u and v variables, while \mathcal{L}_2 is only a function of u . Let us denote $(\bar{\alpha}_1 u, \bar{\alpha}_2 v)$, $\bar{\lambda} u$ and $(\bar{\gamma}_1 u, \bar{\gamma}_2 v)$ the associated linearized parts of the \mathcal{L}_1 , \mathcal{L}_2 and \mathcal{L}_3 operators with respect to the (u, v) variables, respectively. We will consider that all these factors are real numbers. The linearized system can then be written as

$$\begin{cases} u_t = \bar{\alpha}_1 u + \bar{\alpha}_2 v, \\ v_t = \bar{\gamma}_1 u + \bar{\gamma}_2 v + \bar{\lambda} u, \end{cases} \quad (10)$$

which in matrix form reads

$$U_t = AU \quad ; \quad U \equiv \begin{pmatrix} u \\ v \end{pmatrix} \quad ; \quad A = \begin{pmatrix} \bar{\alpha}_1 & \bar{\alpha}_2 \\ \bar{\gamma}_1 + \bar{\lambda} & \bar{\gamma}_2 \end{pmatrix}. \quad (11)$$

The eigenvalues of A are

$$\sigma_{\pm} = \frac{1}{2} \left[\bar{\alpha}_1 + \bar{\gamma}_2 \pm \sqrt{(\bar{\alpha}_1 - \bar{\gamma}_2)^2 + 4\bar{\alpha}_2(\bar{\gamma}_1 + \bar{\lambda})} \right]. \quad (12)$$

Given that the coefficients are real, wave-like solutions of these equations (or oscillatory solutions for the case of ODEs) appear if the eigenvalues have a non vanishing imaginary part.

Definition 2.1. The system (9), whose linear part has the form (10), is said to be a system of *wave-like equations* if

$$(\bar{\alpha}_1 - \bar{\gamma}_2)^2 + 4\bar{\alpha}_2(\bar{\gamma}_1 + \bar{\lambda}) < 0. \quad (13)$$

A system of wave-like equations can be viewed as a generalisation of a second-order PDE wave equation when written as a first-order system in time. Note that, as a consequence of previous definition, $\bar{\alpha}_2(\bar{\gamma}_1 + \bar{\lambda}) < 0$ is a necessary condition for the system to be of wave-like equations.

Our aim is to deal with systems in which the terms responsible for the wave-like properties appear in the \mathcal{L}_3 operator. Keeping this in mind, we introduce the following definition:

Definition 2.2. The system (9), whose linear part has the form (10), is said to be a system of *separable wave-like equations* if it is a system of *wave-like equations* (definition 2.1) and $\bar{\alpha}_2 \bar{\lambda} < 0$.

The adjective *separable* is used here to indicate that it is possible to separate the differential operator for $\partial_t v$ in such a way that $\bar{\alpha}_2 \bar{\lambda} < 0$. As we show in the numerical examples of Sects. 5 to 7, this condition is fairly easily fulfilled in typical examples of *wave-like equations*. The property of *separable wave-like equations* is of help in the next sections for the stability analysis of the PIRK methods.

3. Partially implicit Runge-Kutta methods

Let us consider a discretisation of the differential operators \mathcal{L}_1 , \mathcal{L}_2 and \mathcal{L}_3 , appearing in a system of separable wave-like equations of the form (9), which we denote by L_1 , L_2 and L_3 , respectively. No restrictions onto the discrete operators are imposed. Following the philosophy of the semi-implicit Euler method we want to build methods in which L_1 and L_3 are treated in an explicit way, whereas the L_2 operator is treated implicitly, and contains the terms responsible for the numerical instabilities.

Definition 3.1. We define a *partially implicit Runge Kutta* (PIRK) scheme as a numerical integration scheme in which:

1. The variable u is evolved explicitly by means of a ERK scheme. Each stage of the ERK for u corresponds to a stage of the PIRK scheme.
2. In each stage of the PIRK method, the variable v is evolved taking into account the updated value of u for the evaluation of the L_2 operator.

3. The evaluation of L_1 , L_2 and L_3 at each stage is performed at the same time level.
4. If $\mathcal{L}_2 = 0$ an ERK scheme is recovered.

The general structure of a PIRK method to integrate t from t^n to $t^{n+1} = t^n + \Delta t$, being Δt the time step, in s stages is the following one:

$$\begin{cases} u^{(0)} = u^n, \\ v^{(0)} = v^n, \end{cases} \quad (14)$$

where u^n and v^n are the values of the variables at t^n ; for the intermediate stages $i = 1, \dots, s-1$, intermediate variables can be computed as

$$\begin{cases} u^{(i)} = u^n + \Delta t \sum_{j=0}^{i-1} a_{i+1j+1} L_1(t^{(j)}, u^{(j)}, v^{(j)}), \\ v^{(i)} = v^n + \Delta t \sum_{j=0}^i \tilde{a}_{i+1j+1} L_2(t^{(j)}, u^{(j)}) + \Delta t \sum_{j=0}^{i-1} a_{i+1j+1} L_3(t^{(j)}, u^{(j)}, v^{(j)}), \end{cases} \quad (15)$$

where $t^{(j)} \equiv t^n + c_{j+1}\Delta t$; finally, the values of the variables at t^{n+1} are

$$\begin{cases} u^{n+1} = u^{(s)} = u^n + \Delta t \sum_{j=0}^{s-1} b_{j+1} L_1(t^{(j)}, u^{(j)}, v^{(j)}), \\ v^{n+1} = v^{(s)} = v^n + \Delta t \sum_{j=0}^s \tilde{b}_{j+1} L_2(t^{(j)}, u^{(j)}) + \Delta t \sum_{j=0}^{s-1} b_{j+1} L_3(t^{(j)}, u^{(j)}, v^{(j)}), \end{cases} \quad (16)$$

where the coefficients a_{ij} , \tilde{a}_{ij} , b_j and \tilde{b}_j are real constants and

$$c_i = \sum_{j=1}^s a_{ij}. \quad (17)$$

The coefficients a_{ij} , b_j and c_i , with $i, j = 1, \dots, s$, correspond to the coefficients of a Butcher tableau (see e.g. [1]) for an ERK scheme with s stages. These coefficients appear only in front of L_1 and L_3 operators. Therefore, if $L_2 = 0$ the method is equivalent to an ERK.

The coefficients \tilde{a}_{ij} and \tilde{b}_j , in front of L_2 operator, do not correspond to a s -stages RK method because, in general, there is a non-zero \tilde{b}_{s+1} coefficient. However, they correspond to a diagonally implicit RK (DIRK, see e.g. [1]) method of $s+1$ stages, where $\tilde{a}_{s+1j} = \tilde{b}_j$ and $\tilde{c}_i = c_i$. The latter condition is necessary to fulfill the condition that all operators are computed at the same time level, $t^{(i)}$, when evaluated at a given stage i . In general, a PIRK method of s stages can be written as a particular case of an IMEX RK method with $s+1$ stages with the Butcher's tableau given in table 1. Note that the explicit part is formally extended to $s+1$ stages by adding an additional trivial step in the $s+1$ row.

By using this structure it is possible to evaluate the L_2 operator at each stage using previously computed values of $u^{(j)}$, without the need of any analytical or numerical inversion of operators. This strategy results in a numerical method which is explicit in this sense and hence comparable in computational cost to ERK schemes. Note that the PIRK methods can be trivially generalised to systems of 3 or more equations by considering variables u and v as vectors of variables.

Although the method, viewed as a IMEX-RK scheme, has $s+1$ stages, in practice it is only necessary to compute each L_i operator, $i = 1, 2, 3$, s times per iteration. The reason is that the computation of $L_2(u^{(0)}) = L_2(u^n)$ coincides with the value of $L_2(u^{(s)})$ at the previous iteration, so it is necessary to compute $s+1$ stages only in the first iteration. Therefore, we denote this method as a PIRK one with s stages.

Table 1: Tableau for the explicit (left) and the implicit (right) part of a general PIRK scheme written as an IMEX-RK one.

0	0	0	0	...	0	0	0	0	0	0	...	0	0
c_2	a_{21}	0	0	...	0	0	c_2	\tilde{a}_{21}	\tilde{a}_{22}	0	...	0	0
c_3	a_{31}	a_{32}	0	...	0	0	c_3	\tilde{a}_{31}	\tilde{a}_{32}	\tilde{a}_{33}	...	0	0
\vdots	\vdots	\vdots	\ddots	...	\vdots	\vdots	\vdots	\vdots	\ddots	...	\vdots	\vdots	
c_s	a_{s1}	a_{s2}	...	$a_{s,s-1}$	0	0	c_s	\tilde{a}_{s1}	\tilde{a}_{s2}	...	$\tilde{a}_{s,s-1}$	\tilde{a}_{ss}	0
1	b_1	b_2	...	b_{s-1}	b_s	0	1	\tilde{b}_1	\tilde{b}_2	...	\tilde{b}_{s-1}	\tilde{b}_s	\tilde{b}_{s+1}
	b_1	b_2	...	b_{s-1}	b_s	0		\tilde{b}_1	\tilde{b}_2	...	\tilde{b}_{s-1}	\tilde{b}_s	\tilde{b}_{s+1}

4. Numerical methods and stability analysis

In this section we derive the PIRK methods up to fourth-order. We construct methods of first, second and third-order with one, two and three stages, respectively. For the fourth-order scheme we use five stages. To fix all the coefficients of the PIRK methods described in the previous section, we follow the following procedure:

- i) We choose the coefficients a_{ij} and b_j to recover the optimal SSP ERK method when implicitly treated parts are neglected (i.e. when $L_2 = 0$).
- ii) We choose the coefficients \tilde{a}_{ij} and \tilde{b}_j such that the implicit part fulfills the conditions of a DIRK scheme. This step imposes restrictions over the possible values of the \tilde{a}_{ij} and \tilde{b}_j coefficients.
- iii) We choose the remaining free coefficients optimising the stability properties of the numerical scheme.

4.1. Explicit part

Numerical methods based on a nonlinear stability requirement are very desirable. For this reason we choose strong stability preserving (SSP) methods (see e.g. [24, 25]) for the explicit part of our PIRK schemes. Forward Euler method corresponds to the first-order optimal SSP method. Gottlieb and Shu [24] proved that the classical second-order (Heun's) method,

$$\begin{aligned}
 U^{(0)} &= U^n, \\
 U^{(1)} &= U^n + \Delta t L(U^n), \\
 U^{n+1} &= \frac{1}{2}U^n + \frac{1}{2}U^{(1)} + \frac{1}{2}\Delta t L(U^{(1)}),
 \end{aligned} \tag{18}$$

is the optimal second-order two-stage SSP ERK method (ERK2 hereafter), and that the third-order method due to Shu and Osher [26],

$$\begin{aligned}
 U^{(0)} &= U^n, \\
 U^{(1)} &= U^n + \Delta t L(U^n), \\
 U^{(2)} &= \frac{3}{4}U^n + \frac{1}{4}U^{(1)} + \frac{1}{4}\Delta t L(U^{(1)}), \\
 U^{n+1} &= \frac{1}{3}U^n + \frac{2}{3}U^{(2)} + \frac{2}{3}\Delta t L(U^{(2)}),
 \end{aligned} \tag{19}$$

is the optimal third-order three-stage SSP ERK method (ERK3 hereafter). The optimal adjective, for a given number of stages, refers to a maximization of the corresponding Courant-Friedrichs-Lewy (CFL) value (1 in both cases) and the efficiency in the storage requirement. This property is crucial to capture the

right behavior of the evolution of the system. The fourth-order five-stage optimal SSP ERK with positive coefficients was found in [27] and again independently in [28], and guaranteed optimal [29] (ERK4 hereafter); it has the following form:

$$\begin{aligned}
U^{(0)} &= U^n, \\
U^{(1)} &= U^n + 0.391752226571890 \Delta t L(U^n), \\
U^{(2)} &= 0.444370493651235 U^n \\
&\quad + 0.555629506348765 U^{(1)} + 0.368410593050371 \Delta t L(U^{(1)}), \\
U^{(3)} &= 0.620101851488403 U^n \\
&\quad + 0.379898148511597 U^{(2)} + 0.251891774271694 \Delta t L(U^{(2)}), \\
U^{(4)} &= 0.178079954393132 U^n \\
&\quad + 0.821920045606868 U^{(3)} + 0.544974750228521 \Delta t L(U^{(3)}), \\
U^{n+1} &= 0.517231671970585 U^{(2)} \\
&\quad + 0.096059710526147 U^{(3)} + 0.063692468666290 \Delta t L(U^{(3)}) \\
&\quad + 0.386708617503269 U^{(4)} + 0.226007483236906 \Delta t L(U^{(4)}). \tag{20}
\end{aligned}$$

We use these SSP ERK methods for the explicit part of the PIRK schemes. Therefore the stability properties of the PIRK methods, when $L_2 = 0$, are the same as those of the SSP methods, which guarantees a good stability properties of the explicit part. In the next sections we assume that the numerical method, applied to the system at hand, is stable when $L_2 = 0$.

Let us consider the linearized system (10). The first step in all SSP ERK methods mentioned above for the explicit part of the system of equations (i.e. when $L_2 = 0$ or equivalently $\bar{\lambda} = 0$) can be written as

$$\begin{pmatrix} u \\ v \end{pmatrix}^{n+1} = \begin{pmatrix} 1 + \alpha_1 & \alpha_2 \\ \gamma_1 & 1 + \gamma_2 \end{pmatrix} \begin{pmatrix} u \\ v \end{pmatrix}^n, \tag{21}$$

where $\alpha_i := \bar{\alpha}_i \Delta t$ and $\gamma_i := \bar{\gamma}_i \Delta t$. For completeness and later use we also define $\lambda := \bar{\lambda} \Delta t$. The matrix appearing in the previous equation is referred as the stability matrix. Let us denote ω_i , $i = 1, 2$, its two eigenvalues. As we are assuming that the explicit part of the system is numerically stable, it is necessary that $|\omega_i| \leq 1$. Let us denote by dex and trex the determinant and trace of the stability matrix of the explicit part, respectively. The condition $|\omega_i| \leq 1$ implies, in particular, that these quantities are bounded as

$$\text{dex} = |\omega_1| |\omega_2| = |(1 + \alpha_1)(1 + \gamma_2) - \alpha_2 \gamma_1| \leq 1, \tag{22}$$

$$\text{trex} = |\omega_1 + \omega_2| = |2 + \alpha_1 + \gamma_2| \leq 2. \tag{23}$$

We use this property of the explicit part in the next sections to ensure the stability of the PIRK methods.

4.2. Stability considerations

We consider next the stability properties of the PIRK methods once the implicit part is included. We focus here on the linear stability of the system; the analysis of the linear stability is the most simple case regarding the study of the stability of a system of equations, but if a method does not verify even this criteria it is obviously not stable in general. In most cases, the linear part of the system is the dominant one and the results obtained in the analysis of the linear stability are reproduced in the numerical simulations.

Since we are considering a system of equations and the characteristic structure of eigenvalues and eigenvectors of the explicit and implicit parts do not coincide necessarily, we have to consider the global structure of the system and the analysis has to involve the matrices which update the variables from one time step to the next one.

Let us denote by M_i the matrix which updates values of the variables for a i th-order PIRK method,

$$\begin{pmatrix} u^{n+1} \\ v^{n+1} \end{pmatrix} = M_i \begin{pmatrix} u^n \\ v^n \end{pmatrix}. \tag{24}$$

Linear stability thus requires that the absolute value of the two eigenvalues associated to the matrix M_i are bounded by 1. However, in order to simplify the derivation of the PIRK methods, we are going to relax this condition on the eigenvalues of the matrix M_i by a bound on its determinant, $|\det(M_i)| \leq 1$. The idea is to restrict in a very effective way the possible range of values for the remaining coefficients associated to the implicit operator; moreover, in the numerical examples of the next sections, we will show that the optimal values for the coefficients are very close or equal to the ones found when the bound on the determinant is used. The different restrictions coming from both the bound of the determinant (boundary of the stability region) and the eigenvalues will be shown in some of the numerical experiments (see Sect. 6).

Since we are considering systems of separable wave-like equations (see definition 2.2), we can assume that $\lambda\alpha_2 < 0$ (see numerical examples in the following sections). The combination $\lambda\alpha_2$ will appear in numerous places and basically counts for the freedom in the definition of the variable v up to a constant factor, without changing the nature of the system of equations. This quantity is not necessarily very large, since we are not considering here that this source term is stiff in this sense; we will consider in our analysis the cases $|\lambda\alpha_2| \ll 1$, $\lambda\alpha_2 \approx -1$ and $|\lambda\alpha_2| \gg 1$, in order to check the validity of the derived methods in all the possible ranges.

4.3. First-order method

A one-stage first-order PIRK method for a separable wave-like equation can be written in general as

$$\begin{cases} u^{n+1} = u^n + \Delta t L_1(u^n, v^n), \\ v^{n+1} = v^n + \Delta t [(1 - \mathcal{C}_1)L_2(u^n) + \mathcal{C}_1 L_2(u^{n+1}) + L_3(u^n, v^n)], \end{cases} \quad (25)$$

where \mathcal{C}_1 , a real constant, is the only free parameter. This method is a particular case for the system (9) of the so-called IMEX- θ method (see e.g. [32]), where \mathcal{C}_1 is the θ parameter. According to [32], \mathcal{C}_1 must be chosen such that $\mathcal{C}_1 \geq 1/2$.

System (25) can be written as

$$\begin{pmatrix} u^{n+1} \\ v^{n+1} \end{pmatrix} = M_1 \begin{pmatrix} u^n \\ v^n \end{pmatrix}, \quad (26)$$

where

$$M_1 = \begin{pmatrix} 1 + \alpha_1 & \alpha_2 \\ \gamma_1 + \lambda(1 + \alpha_1\mathcal{C}_1) & 1 + \gamma_2 + \lambda\alpha_2\mathcal{C}_1 \end{pmatrix}. \quad (27)$$

Since $\det(M_1) = \det(\lambda\alpha_2(1 - \mathcal{C}_1))$ and taking into account the condition (22), the only value of \mathcal{C}_1 which guarantees $|\det(M_1)| \leq 1 \forall (\lambda\alpha_2)$ is $\mathcal{C}_1 = 1$. This value satisfies the condition $\mathcal{C}_1 \geq 1/2$. The resulting method is:

$$\begin{cases} u^{n+1} = u^n + \Delta t L_1(u^n, v^n), \\ v^{n+1} = v^n + \Delta t [L_2(u^{n+1}) + L_3(u^n, v^n)]. \end{cases} \quad (28)$$

This method, which we call PIRK1 hereafter, is well known in the literature as the ARS(1,1,1) method [3, 2]. For the case $L_3 = 0$ it coincides with the semi-implicit Euler method. Table 2 shows the tableau of the PIRK1 method expressed as an 2 stages IMEX-RK one. The derivation of the PIRK1 scheme is presented here as an illustration of the procedure we want to follow to derive higher-order PIRK methods.

4.4. Second-order method

Next we derive a two-stages second-order PIRK method (PIRK2 hereafter), which can be regarded as an IMEX-RK scheme with three-stages. We impose the two-stages second-order SSP optimal method for the purely explicit parts (L_1 and L_3 operators). The remaining coefficients are restricted by the order conditions (see [31] for second-order and $s = 3$) and $c_i = \tilde{c}_i$ (but $b_i \neq \tilde{b}_i$ in general). With these conditions, the PIRK2 method can be written in terms of two free real coefficients, $(\mathcal{C}_1, \mathcal{C}_2)$, as follows:

$$\begin{cases} u^{(1)} = u^n + \Delta t L_1(u^n, v^n), \\ v^{(1)} = v^n + \Delta t [(1 - \mathcal{C}_1)L_2(u^n) + \mathcal{C}_1 L_2(u^{(1)}) + L_3(u^n, v^n)], \end{cases} \quad (29)$$

Table 2: Tableau for the explicit (left) and implicit (right) part of a general one-stage first-order PIRK method, expressed as an 2 stages IMEX-RK scheme. Values of \mathcal{C}_1 for different schemes are also given.

0	0	0	0	0	0
1	1	0	1	$1 - \mathcal{C}_1$	\mathcal{C}_1
1	0		1	$1 - \mathcal{C}_1$	\mathcal{C}_1
PIRK1: $\mathcal{C}_1 = 1$.					
ERK1 (forward Euler): $\mathcal{C}_1 = 0$.					

$$\begin{cases} u^{n+1} = \frac{1}{2} \left[u^n + u^{(1)} + \Delta t L_1(u^{(1)}, v^{(1)}) \right], \\ v^{n+1} = v^n + \frac{\Delta t}{2} \left[L_2(u^n) + 2\mathcal{C}_2 L_2(u^{(1)}) + (1 - 2\mathcal{C}_2) L_2(u^{n+1}) \right. \\ \left. + L_3(u^n, v^n) + L_3(u^{(1)}, v^{(1)}) \right]. \end{cases} \quad (30)$$

From (29) and (30),

$$\begin{pmatrix} u^{n+1} \\ v^{n+1} \end{pmatrix} = M_2 \begin{pmatrix} u^n \\ v^n \end{pmatrix}, \quad (31)$$

where

$$\begin{aligned} M_2 = & \begin{pmatrix} 1 & 0 \\ (1/2 - \mathcal{C}_2)\lambda & 1 \end{pmatrix} \left[\begin{pmatrix} 1/2 & 0 \\ (\lambda + \gamma_1)/2 & 1 + \gamma_2/2 \end{pmatrix} \right. \\ & \left. + \frac{1}{2} \begin{pmatrix} 1 + \alpha_1 & \alpha_2 \\ \gamma_1 + 2\lambda\mathcal{C}_2 & \gamma_2 \end{pmatrix} \begin{pmatrix} 1 + \alpha_1 & \alpha_2 \\ \gamma_1 + \lambda(1 + \alpha_1\mathcal{C}_1) & 1 + \gamma_2 + \lambda\alpha_2\mathcal{C}_1 \end{pmatrix} \right]. \end{aligned} \quad (32)$$

Its determinant is given by:

$$\begin{aligned} \det(M_2) = & \frac{1}{4} \left[(1 - \text{dex})^2 + \text{trex}^2 + \lambda\alpha_2(1 - \text{dex})(1 - 2\mathcal{C}_1 + 2\mathcal{C}_2) \right. \\ & \left. + (\lambda\alpha_2)^2(2\mathcal{C}_2 - \mathcal{C}_1 - 2\mathcal{C}_1\mathcal{C}_2) \right]. \end{aligned} \quad (33)$$

The conditions $1 - 2\mathcal{C}_1 + 2\mathcal{C}_2 = 2\mathcal{C}_2 - \mathcal{C}_1 - 2\mathcal{C}_1\mathcal{C}_2 = 0$ guarantee $|\det(M_2)| \leq 1 \forall (\lambda\alpha_2)$, but they lead to $\mathcal{C}_1 = (1 \pm i)/2 \notin \mathbb{R}$, $\mathcal{C}_2 = \pm i/2 \notin \mathbb{R}$, where $i = \sqrt{-1}$ is the imaginary unit. The condition on the bound for the determinant of M_2 , $|\det(M_2)| \leq 1$, is equivalent to:

$$-4 \leq K_1 + \lambda\alpha_2 K_2(1 - 2\mathcal{C}_1 + 2\mathcal{C}_2) + (\lambda\alpha_2)^2(2\mathcal{C}_2 - \mathcal{C}_1 - 2\mathcal{C}_1\mathcal{C}_2) \leq 4, \quad (34)$$

where

$$K_1 := (1 - \text{dex})^2 + \text{trex}^2 = 1 + \omega_1^2\omega_2^2 + \omega_1^2 + \omega_2^2 \in [1, 4] \quad (35)$$

and

$$K_2 := 1 - \text{dex} \in [0, 2]. \quad (36)$$

The minimum value of K_1 is reached for $\omega_1 = \omega_2 = 0$. The maximum value of K_1 is reached for $\omega_1^2 = \omega_2^2 = 1$. The minimum value of K_2 is reached for $\omega_1 = \omega_2 = \pm 1$. The maximum value of K_2 is reached for $\omega_1 = -\omega_2 = \pm 1$. For $\omega_1 = \omega_2 = 0$, $K_2 = 1$. We analyse the value of $\det(M_2)$ for $\omega_i = 0, \pm 1$, $i = 1, 2$, and in the cases $|\lambda\alpha_2| \ll 1$, $\lambda\alpha_2 \approx -1$ and $|\lambda\alpha_2| \gg 1$. The resulting sufficient conditions are (see Appendix A for more details):

$$\begin{aligned} 0 \leq & 2\mathcal{C}_2(1 - \mathcal{C}_1) - \mathcal{C}_1, \quad 1 - 2\mathcal{C}_1 + 2\mathcal{C}_2 \leq 0, \\ 0 \leq & 6 + 5\mathcal{C}_1 - 6\mathcal{C}_2 + 2\mathcal{C}_1\mathcal{C}_2, \quad 0 \leq 4 + \mathcal{C}_1 - 2\mathcal{C}_1\mathcal{C}_2, \end{aligned} \quad (37)$$

Table 3: Tableau for the explicit (left) and implicit (right) part of a general 2 stages second-order PIRK method, expressed as a 3 stages IMEX-RK scheme. Values of \mathcal{C}_1 and \mathcal{C}_2 for different particular schemes are also given.

0	0	0	0	0	0	0	0
1	1	0	0	1	$1 - \mathcal{C}_1$	\mathcal{C}_1	0
1	$1/2$	$1/2$	0	1	$1/2$	\mathcal{C}_2	$1/2 - \mathcal{C}_2$
	$1/2$	$1/2$	0		$1/2$	\mathcal{C}_2	$1/2 - \mathcal{C}_2$
PIRK2a: $(\mathcal{C}_1, \mathcal{C}_2) = (1/2, 0)$							
PIRK2b: $(\mathcal{C}_1, \mathcal{C}_2) = (1 - \sqrt{2}/2, (\sqrt{2} - 1)/2)$							
ERK2 (Heun's): $(\mathcal{C}_1, \mathcal{C}_2) = (0, 1/2)$							

which involve only coefficients \mathcal{C}_i , together with

$$-4 \leq \lambda\alpha_2(1 - 2\mathcal{C}_1 + 2\mathcal{C}_2), \quad -5 \leq (\lambda\alpha_2)^2(2\mathcal{C}_2 - \mathcal{C}_1 - 2\mathcal{C}_1\mathcal{C}_2). \quad (38)$$

For $|\lambda\alpha_2| \ll 1$, the first inequality in (38) is the most relevant one. We impose $1 - 2\mathcal{C}_1 + 2\mathcal{C}_2 = 0$, and minimize $|2\mathcal{C}_2(1 - \mathcal{C}_1) - \mathcal{C}_1|$ (taking into account (37)). The resulting values for the coefficients are $\mathcal{C}_1 = 1/2$ and $\mathcal{C}_2 = 0$. The scheme, which we will call PIRK2a hereafter, is then written as:

$$\begin{cases} u^{(1)} = u^n + \Delta t L_1(u^n, v^n), \\ v^{(1)} = v^n + \Delta t \left[\frac{1}{2}L_2(u^n) + \frac{1}{2}L_2(u^{(1)}) + L_3(u^n, v^n) \right], \end{cases} \quad (39)$$

$$\begin{cases} u^{n+1} = \frac{1}{2} \left[u^n + u^{(1)} + \Delta t L_1(u^{(1)}, v^{(1)}) \right], \\ v^{n+1} = v^n + \frac{\Delta t}{2} \left[L_2(u^n) + L_2(u^{n+1}) + L_3(u^n, v^n) + L_3(u^{(1)}, v^{(1)}) \right]. \end{cases} \quad (40)$$

For $|\lambda\alpha_2| \gg 1$, second inequality in (38) is the most relevant one. We impose $2\mathcal{C}_2 - \mathcal{C}_1 - 2\mathcal{C}_1\mathcal{C}_2 = 0$, and minimize $|1 - 2\mathcal{C}_1 + 2\mathcal{C}_2|$ (taking into account (37)). The resulting values for the coefficients are $\mathcal{C}_1 = 1 - \sqrt{2}/2$ and $\mathcal{C}_2 = (\sqrt{2} - 1)/2$. The scheme, named PIRK2b hereafter, is written in this case as:

$$\begin{cases} u^{(1)} = u^n + \Delta t L_1(u^n, v^n), \\ v^{(1)} = v^n + \Delta t \left[\frac{\sqrt{2}}{2}L_2(u^n) + \left(1 - \frac{\sqrt{2}}{2}\right)L_2(u^{(1)}) + L_3(u^n, v^n) \right], \end{cases} \quad (41)$$

$$\begin{cases} u^{n+1} = \frac{1}{2} \left[u^n + u^{(1)} + \Delta t L_1(u^{(1)}, v^{(1)}) \right], \\ v^{n+1} = v^n + \frac{\Delta t}{2} \left[L_2(u^n) + (\sqrt{2} - 1)L_2(u^{(1)}) + (2 - \sqrt{2})L_2(u^{n+1}) \right. \\ \left. + L_3(u^n, v^n) + L_3(u^{(1)}, v^{(1)}) \right]. \end{cases} \quad (42)$$

Depending of the value of $|\lambda\alpha_2|$, it will be more convenient to use a particular set of values for the coefficients. This fact will be illustrated in numerical examples of Sects. 5 and 6. Table 3 shows the tableau of the second-order PIRK method expressed as a 3 stages IMEX-RK scheme.

4.5. Third-order method

The three-stages third-order PIRK method can be viewed as a four-stages IMEX-RK scheme. For the purely explicit parts ($L1$ and $L3$ operators) we impose the SSP optimal three-stages third-order method. The remaining coefficients are restricted by the order conditions (see [31] for third-order and $s = 4$) and

$c_i = \tilde{c}_i$ (but $b_i \neq \tilde{b}_i$ in general). The resulting method can be written in terms of two real coefficients, $(\mathcal{C}_1, \mathcal{C}_2)$ (do not confuse these coefficients with the ones appearing in previous methods), as follows:

$$\begin{cases} u^{(1)} = u^n + \Delta t L_1(u^n, v^n), \\ v^{(1)} = v^n + \Delta t \left[(1 - \mathcal{C}_1)L_2(u^n) + \mathcal{C}_1 L_2(u^{(1)}) + L_3(u^n, v^n) \right], \end{cases} \quad (43)$$

$$\begin{cases} u^{(2)} = \frac{1}{4} \left[3u^n + u^{(1)} + \Delta t L_1(u^{(1)}, v^{(1)}) \right], \\ v^{(2)} = v^n + \frac{\Delta t}{4} \left[2(\mathcal{C}_1 + 2\mathcal{C}_2)L_2(u^n) + 4\mathcal{C}_2 L_2(u^{(1)}) + 2(1 - \mathcal{C}_1 - 4\mathcal{C}_2)L_2(u^{(2)}) \right. \\ \left. + L_3(u^n, v^n) + L_3(u^{(1)}, v^{(1)}) \right], \end{cases} \quad (44)$$

$$\begin{cases} u^{n+1} = \frac{1}{3} \left[u^n + 2u^{(2)} + 2\Delta t L_1(u^{(2)}, v^{(2)}) \right], \\ v^{n+1} = v^n + \frac{\Delta t}{6} \left[L_2(u^n) + L_2(u^{(1)}) + 4L_2(u^{(2)}) \right. \\ \left. + L_3(u^n, v^n) + L_3(u^{(1)}, v^{(1)}) + 4L_3(u^{(2)}, v^{(2)}) \right], \end{cases} \quad (45)$$

From (43)-(45),

$$\begin{pmatrix} u^{n+1} \\ v^{n+1} \end{pmatrix} = M_3 \begin{pmatrix} u^n \\ v^n \end{pmatrix}, \quad (46)$$

where

$$M_3 = \begin{pmatrix} 1 + \frac{\alpha_1}{6} & \frac{\alpha_2}{6} \\ \frac{\gamma_1 + \lambda}{6} & 1 + \frac{\gamma_2}{6} \end{pmatrix} + \begin{pmatrix} \alpha_1 & \alpha_2 \\ \gamma_1 + \lambda & \gamma_2 \end{pmatrix} \left(\frac{1}{6}N_1 + \frac{2}{3}N_2 \right), \quad (47)$$

$$N_1 = \begin{pmatrix} 1 & 0 \\ \lambda\mathcal{C}_1 & 1 \end{pmatrix} \begin{pmatrix} 1 + \alpha_1 & \alpha_2 \\ \gamma_1 + \lambda(1 - \mathcal{C}_1) & 1 + \gamma_2 \end{pmatrix}, \quad (48)$$

$$N_2 = \begin{pmatrix} 1 & 0 \\ (1 - \mathcal{C}_1 - 4\mathcal{C}_2)\frac{\lambda}{2} & 1 \end{pmatrix} \left[\begin{pmatrix} 1 + \frac{\alpha_1}{4} & \frac{\alpha_2}{4} \\ \frac{\gamma_1}{4} + (\mathcal{C}_1 + 2\mathcal{C}_2)\frac{\lambda}{2} & 1 + \frac{\gamma_2}{4} \end{pmatrix} + \begin{pmatrix} \frac{\alpha_1}{4} & \frac{\alpha_2}{4} \\ \frac{\gamma_1}{4} + \lambda\mathcal{C}_2 & \frac{\gamma_2}{4} \end{pmatrix} N_1 \right]. \quad (49)$$

Its determinant is given by:

$$\begin{aligned} \det(M_3) &= \frac{1}{36} \left[14 + 2(\text{trex} - 1)^3 + (\text{dex} - 2)^3 + 6 \text{trex}^2 + 3 \text{dex}((\text{trex} - 1)^2 - 2) \right] \\ &+ \frac{1}{24} \lambda \alpha_2 (-1 + \mathcal{C}_1 - 4\mathcal{C}_2) \left[(\text{dex} - 2)^2 + (\text{trex} - 1)^2 - 2 \right] \\ &+ \frac{1}{12} (\lambda \alpha_2)^2 \left[\mathcal{C}_1 - 4\mathcal{C}_2 + (\text{dex} - 1)(4\mathcal{C}_2 - \mathcal{C}_1^2 - 4\mathcal{C}_1\mathcal{C}_2) \right] \\ &- \frac{1}{72} (\lambda \alpha_2)^3 \left[-1 + 3(1 - 2\mathcal{C}_1)(\mathcal{C}_1 + 4\mathcal{C}_2) \right]. \end{aligned} \quad (50)$$

The expressions $-1 + \mathcal{C}_1 - 4\mathcal{C}_2$, $\mathcal{C}_1 - 4\mathcal{C}_2$, $4\mathcal{C}_2 - \mathcal{C}_1^2 - 4\mathcal{C}_1\mathcal{C}_2$ and $-1 + 3(1 - 2\mathcal{C}_1)(\mathcal{C}_1 + 4\mathcal{C}_2)$ cannot vanish simultaneously. The condition $|\det(M_3)| \leq 1$ is equivalent to:

$$\begin{aligned} -1 &\leq \frac{K_3}{36} + \frac{\lambda \alpha_2 K_4 (-1 + \mathcal{C}_1 - 4\mathcal{C}_2)}{24} \\ &+ \frac{(\lambda \alpha_2)^2}{12} \left[\mathcal{C}_1 - 4\mathcal{C}_2 + (\text{dex} - 1)(4\mathcal{C}_2 - \mathcal{C}_1^2 - 4\mathcal{C}_1\mathcal{C}_2) \right] \\ &- \frac{(\lambda \alpha_2)^3}{72} \left[-1 + 3(1 - 2\mathcal{C}_1)(\mathcal{C}_1 + 4\mathcal{C}_2) \right] \leq 1, \end{aligned} \quad (51)$$

where

$$K_3 := 14 + 2(\text{trex} - 1)^3 + (\text{dex} - 2)^3 + 6\text{trex}^2 + 3\text{dex}[(\text{trex} - 1)^2 - 2] \in [-12, 36], \quad (52)$$

and

$$K_4 := (\text{dex} - 2)^2 + (\text{trex} - 1)^2 - 2 \in [0, 8]. \quad (53)$$

The minimum value of K_3 is reached for $\omega_1 = 1 = -\omega_2$ and $\omega_2 = 1 = -\omega_1$. For $\omega_1 = \omega_2 = -1$, $K_3 = 4$. The maximum value of K_3 is reached for $\omega_1 = \omega_2 = 1$. The minimum value of K_4 is reached for $\omega_1 = \omega_2 = 1$. The maximum value of K_4 is reached for $\omega_1 = \omega_2 = -1$, $\omega_1 = 1 = -\omega_2$ and $\omega_2 = 1 = -\omega_1$.

We analyse the bound for the determinant for the values $\omega_i = \pm 1$, $i = 1, 2$, and in the cases $|\lambda\alpha_2| \ll 1$, $\lambda\alpha_2 \approx -1$ and $|\lambda\alpha_2| \gg 1$. The resulting sufficient conditions are (see Appendix B for more details):

$$\begin{aligned} -\frac{20}{9} \leq \mathcal{C}_1 - 4\mathcal{C}_2 \leq 0, \quad -1 + 3(1 - 2\mathcal{C}_1)(\mathcal{C}_1 + 4\mathcal{C}_2) \leq 0, \\ 0 \leq 73 + 18\mathcal{C}_1^2 - 180\mathcal{C}_2 + 9\mathcal{C}_1(3 + 8\mathcal{C}_2), \quad 0 \leq 9\mathcal{C}_1 - 12\mathcal{C}_2 - 6\mathcal{C}_1^2 - 24\mathcal{C}_1\mathcal{C}_2 + 143, \\ 0 \leq 103 - 15\mathcal{C}_1 - 6\mathcal{C}_1^2 + 84\mathcal{C}_2 - 24\mathcal{C}_1\mathcal{C}_2, \quad 0 \leq 6\mathcal{C}_1^2 - 15\mathcal{C}_1 + 36\mathcal{C}_2 + 24\mathcal{C}_1\mathcal{C}_2 + 71, \end{aligned} \quad (54)$$

which involve only coefficients \mathcal{C}_i , together with

$$\begin{aligned} \lambda\alpha_2(-1 + \mathcal{C}_1 - 4\mathcal{C}_2) \leq \frac{8}{3}, \quad -24 \leq (\lambda\alpha_2)^2(\mathcal{C}_1 - 4\mathcal{C}_2), \\ (\lambda\alpha_2)^3[-1 + 3(1 - 2\mathcal{C}_1)(\mathcal{C}_1 + 4\mathcal{C}_2)] \leq 48. \end{aligned} \quad (55)$$

For $|\lambda\alpha_2| \ll 1$, first inequality in (55) is the most relevant one. Firstly, we minimize $|-1 + \mathcal{C}_1 - 4\mathcal{C}_2|$ (taking into account (54)). Consequently, we choose $\mathcal{C}_2 = \mathcal{C}_1/4$. This condition minimizes the factors accompanying $\lambda\alpha_2$ and $(\lambda\alpha_2)^2$ in (55). The remaining inequalities from (54) and (55) reduce to

$$\frac{3 - \sqrt{1245}}{12} \leq \mathcal{C}_1 \leq \frac{3 + \sqrt{1245}}{12}, \quad (\lambda\alpha_2)^3(-1 + 6\mathcal{C}_1 - 12\mathcal{C}_1^2) \leq 48. \quad (56)$$

Secondly, we minimize $|-1 + 6\mathcal{C}_1 - 12\mathcal{C}_1^2|$ (taking into account its allowed range). The minimum is placed at $\mathcal{C}_1 = 1/4$. Therefore, the resulting values are

$$(\mathcal{C}_1, \mathcal{C}_2) = \left(\frac{1}{4}, \frac{1}{16} \right), \quad (57)$$

and the method, which we call PIRK3a hereafter, is written as

$$\begin{cases} u^{(1)} = u^n + \Delta t L_1(u^n, v^n), \\ v^{(1)} = v^n + \Delta t \left[\frac{3}{4}L_2(u^n) + \frac{1}{4}L_2(u^{(1)}) + L_3(u^n, v^n) \right], \end{cases} \quad (58)$$

$$\begin{cases} u^{(2)} = \frac{1}{4} \left[3u^n + u^{(1)} + \Delta t L_1(u^{(1)}, v^{(1)}) \right], \\ v^{(2)} = v^n + \frac{\Delta t}{4} \left[\frac{3}{4}L_2(u^n) + \frac{1}{4}L_2(u^{(1)}) + L_2(u^{(2)}) \right. \\ \left. + L_3(u^n, v^n) + L_3(u^{(1)}, v^{(1)}) \right], \end{cases} \quad (59)$$

$$\begin{cases} u^{n+1} = \frac{1}{3} \left[u^n + 2u^{(2)} + 2\Delta t L_1(u^{(2)}, v^{(2)}) \right], \\ v^{n+1} = v^n + \frac{\Delta t}{6} \left[L_2(u^n) + L_2(u^{(1)}) + 4L_2(u^{(2)}) \right. \\ \left. + L_3(u^n, v^n) + L_3(u^{(1)}, v^{(1)}) + 4L_3(u^{(2)}, v^{(2)}) \right]. \end{cases} \quad (60)$$

For $|\lambda\alpha_2| \gg 1$, last inequality in (55) is the most relevant one. Firstly, we minimize $|-1 + 3(1 - 2\mathcal{C}_1)(\mathcal{C}_1 + 4\mathcal{C}_2)|$ (taking into account (54)). Consequently, we choose $\mathcal{C}_2 = \frac{1}{4} \left(\frac{1}{3(1 - 2\mathcal{C}_1)} - \mathcal{C}_1 \right)$. This condition minimizes the factor accompanying $(\lambda\alpha_2)^3$ in (55). The remaining inequalities from (54) and (55) reduce to

$$\frac{-17 - \sqrt{2377}}{72} \leq \mathcal{C}_1 \leq \frac{-17 + \sqrt{2377}}{72}, \quad (61)$$

and

$$\lambda\alpha_2 \left(-1 + \frac{(-1 + 6\mathcal{C}_1 - 12\mathcal{C}_1^2)}{3(2\mathcal{C}_1 - 1)} \right) \leq \frac{8}{3}, \quad 24 \leq (\lambda\alpha_2)^2 \frac{(-1 + 6\mathcal{C}_1 - 12\mathcal{C}_1^2)}{3(2\mathcal{C}_1 - 1)}. \quad (62)$$

Secondly, we minimize $\left| \frac{(-1 + 6\mathcal{C}_1 - 12\mathcal{C}_1^2)}{3(2\mathcal{C}_1 - 1)} \right|$ (taking into account its allowed range). The minimum is placed at $\mathcal{C}_1 = \frac{3 - \sqrt{3}}{6}$. Therefore, the resulting values are

$$(\mathcal{C}_1, \mathcal{C}_2) = \left(\frac{3 - \sqrt{3}}{6}, \frac{-1 + \sqrt{3}}{8} \right), \quad (63)$$

and the method, which we call PIRK3b hereafter, is written as

$$\begin{cases} u^{(1)} = u^n + \Delta t L_1(u^n, v^n), \\ v^{(1)} = v^n + \Delta t \left[\frac{(3 + \sqrt{3})}{6} L_2(u^n) + \frac{(3 - \sqrt{3})}{6} L_2(u^{(1)}) + L_3(u^n, v^n) \right], \end{cases} \quad (64)$$

$$\begin{cases} u^{(2)} = \frac{1}{4} \left[3u^n + u^{(1)} + \Delta t L_1(u^{(1)}, v^{(1)}) \right], \\ v^{(2)} = v^n + \frac{\Delta t}{4} \left[\frac{(3 + \sqrt{3})}{6} L_2(u^n) + \frac{(-1 + \sqrt{3})}{2} L_2(u^{(1)}) + \frac{2}{3} (3 - \sqrt{3}) L_2(u^{(2)}) \right. \\ \left. + L_3(u^n, v^n) + L_3(u^{(1)}, v^{(1)}) \right], \end{cases} \quad (65)$$

$$\begin{cases} u^{n+1} = \frac{1}{3} \left[u^n + 2u^{(2)} + 2\Delta t L_1(u^{(2)}, v^{(2)}) \right], \\ v^{n+1} = v^n + \frac{\Delta t}{6} \left[L_2(u^n) + L_2(u^{(1)}) + 4L_2(u^{(2)}) \right. \\ \left. + L_3(u^n, v^n) + L_3(u^{(1)}, v^{(1)}) + 4L_3(u^{(2)}, v^{(2)}) \right]. \end{cases} \quad (66)$$

As in the second-order PIRK methods, depending on the value of $|\lambda\alpha_2|$, it will be more convenient to use a particular set of values for the coefficients (see numerical examples in Sects. 5 and 6).

Table 4 shows the tableau of the third-order PIRK method expressed as a four-stages IMEX-RK scheme. Note that, unlike first and second-order PIRK methods, the resulting IMEX-RK scheme has actually only 3 stages because $\tilde{b}_4 = 0$, and the tableau could be trivially simplified.

4.6. Fourth-order method

The five-stages fourth-order PIRK method can be viewed as a six-stages IMEX-RK scheme. For the purely explicit parts ($L1$ and $L3$ operators) we impose the SSP optimal five-stages fourth-order method. The remaining coefficients are restricted by the order conditions (see [31] for fourth-order and $s = 6$) and $c_i = \tilde{c}_i$ (but $b_i \neq \tilde{b}_i$ in general). The resulting method can be written in terms of five real coefficients, $\mathcal{C}_i, i = 1, \dots, 5$ (do not confuse these coefficients with the ones appearing in previous methods), as follows:

$$\begin{cases} u^{(1)} = u^n + a_{21} \Delta t L_1(u^n, v^n), \\ v^{(1)} = v^n + \Delta t \left[\tilde{a}_{21} L_2(u^n) + \mathcal{C}_1 L_2(u^{(1)}) + a_{21} L_3(u^n, v^n) \right], \end{cases} \quad (67)$$

Table 4: Tableau for the explicit (left) and implicit (right) part of a general three-stages third-order PIRK method, expressed as a four-stages IMEX-RK scheme. Values of \mathcal{C}_1 and \mathcal{C}_2 for different schemes are also given. Note that the tableau can be trivially simplified into 3 stages. *With these values this tableau is equivalent to the IMEX-SSP3(4,3,3) if applied to the system (9) (see section 4.7).

0	0	0	0	0	0	0	0	0	0	0
1	1	0	0	0	1	$1 - \mathcal{C}_1$	\mathcal{C}_1	0	0	0
1/2	1/4	1/4	0	0	1/2	$(\mathcal{C}_1 + 2\mathcal{C}_2)/2$	\mathcal{C}_2	$(1 - \mathcal{C}_1 - 4\mathcal{C}_2)/2$	0	0
1	1/6	1/6	2/3	0	1	1/6	1/6	2/3	0	0
	1/6	1/6	2/3	0		1/6	1/6	2/3	0	0

$$\text{PIRK3a: } (\mathcal{C}_1, \mathcal{C}_2) = (1/4, 1/16)$$

$$\text{PIRK3b: } (\mathcal{C}_1, \mathcal{C}_2) = ((3 - \sqrt{3})/6, (-1 + \sqrt{3})/8)$$

$$\text{ERK3: } (\mathcal{C}_1, \mathcal{C}_2) = (0, 1/4)$$

$$\text{IMEX-SSP3(4,3,3)*: } (\mathcal{C}_1, \mathcal{C}_2) = (0.24169426078821, (1 - 3\mathcal{C}_1)/4)$$

$$\begin{cases} u^{(2)} = u^n + \Delta t \left[a_{31} L_1(u^n, v^n) + a_{32} L_1(u^{(1)}, v^{(1)}) \right], \\ v^{(2)} = v^n + \Delta t \left[\tilde{a}_{31} L_2(u^n) + \tilde{a}_{32} L_2(u^{(1)}) + \mathcal{C}_2 L_2(u^{(2)}) \right. \\ \left. + a_{31} L_3(u^n, v^n) + a_{32} L_3(u^{(1)}, v^{(1)}) \right], \end{cases} \quad (68)$$

$$\begin{cases} u^{(3)} = u^n + \Delta t \left[a_{41} L_1(u^n, v^n) + a_{42} L_1(u^{(1)}, v^{(1)}) + a_{43} L_1(u^{(2)}, v^{(2)}) \right], \\ v^{(3)} = v^n + \Delta t \left[\tilde{a}_{41} L_2(u^n) + \tilde{a}_{42} L_2(u^{(1)}) + \tilde{a}_{43} L_2(u^{(2)}) + \mathcal{C}_3 L_2(u^{(3)}) \right. \\ \left. + a_{41} L_3(u^n, v^n) + a_{42} L_3(u^{(1)}, v^{(1)}) + a_{43} L_3(u^{(2)}, v^{(2)}) \right], \end{cases} \quad (69)$$

$$\begin{cases} u^{(4)} = u^n + \Delta t \left[a_{51} L_1(u^n, v^n) + a_{52} L_1(u^{(1)}, v^{(1)}) + a_{53} L_1(u^{(2)}, v^{(2)}) \right. \\ \left. + a_{54} L_1(u^{(3)}, v^{(3)}) \right], \\ v^{(4)} = v^n + \Delta t \left[\tilde{a}_{51} L_2(u^n) + \tilde{a}_{52} L_2(u^{(1)}) + \mathcal{C}_4 L_2(u^{(2)}) + \tilde{a}_{54} L_2(u^{(3)}) \right. \\ \left. + \mathcal{C}_5 L_2(u^{(4)}) \right. \\ \left. + a_{51} L_3(u^n, v^n) + a_{52} L_3(u^{(1)}, v^{(1)}) + a_{53} L_3(u^{(2)}, v^{(2)}) \right. \\ \left. + a_{54} L_3(u^{(3)}, v^{(3)}) \right], \end{cases} \quad (70)$$

$$\begin{cases} u^{n+1} = u^n + \Delta t \left[b_1 L_1(u^n, v^n) + b_2 L_1(u^{(1)}, v^{(1)}) + b_3 L_1(u^{(2)}, v^{(2)}) \right. \\ \left. + b_4 L_1(u^{(3)}, v^{(3)}) + b_5 L_1(u^{(4)}, v^{(4)}) \right], \\ v^{n+1} = v^n + \Delta t \left[b_1 L_2(u^n) + b_2 L_2(u^{(1)}) + b_3 L_2(u^{(2)}) \right. \\ \left. + b_4 L_2(u^{(3)}) + b_5 L_2(u^{(4)}) \right. \\ \left. + b_1 L_3(u^n, v^n) + b_2 L_3(u^{(1)}, v^{(1)}) + b_3 L_3(u^{(2)}, v^{(2)}) \right. \\ \left. + b_4 L_3(u^{(3)}, v^{(3)}) + b_5 L_3(u^{(4)}, v^{(4)}) \right], \end{cases} \quad (71)$$

Table 5: Tableau for the explicit (left) and implicit (right) part of a general five-stages fourth-order PIRK method, expressed as a six-stages IMEX-RK scheme. Values of \mathcal{C}_1 and \mathcal{C}_2 for different schemes are also given.

0	0	0	0	0	0	0	0	0	0	0	0	0	0
c_2	a_{21}	0	0	0	0	0	c_2	\tilde{a}_{21}	\mathcal{C}_1	0	0	0	0
c_3	a_{31}	a_{32}	0	0	0	0	c_3	\tilde{a}_{31}	\tilde{a}_{32}	\mathcal{C}_2	0	0	0
c_4	a_{41}	a_{42}	a_{43}	0	0	0	c_4	\tilde{a}_{41}	\tilde{a}_{42}	\tilde{a}_{43}	\mathcal{C}_3	0	0
c_5	a_{51}	a_{52}	a_{53}	a_{54}	0	0	c_5	\tilde{a}_{51}	\tilde{a}_{52}	\mathcal{C}_4	\tilde{a}_{54}	\mathcal{C}_5	0
1	b_1	b_2	b_3	b_4	b_5	0	1	b_1	b_2	b_3	b_4	b_5	0
	b_1	b_2	b_3	b_4	b_5	0		b_1	b_2	b_3	b_4	b_5	0

PIRK4: $(\mathcal{C}_1, \mathcal{C}_2, \mathcal{C}_3, \mathcal{C}_4, \mathcal{C}_5) = (0.13761208339219633, 0.2042433556378285, 0.0904666765339173, 0.3966145239174311, -0.00984245655482246)$
 ERK4: $(\mathcal{C}_1, \mathcal{C}_2, \mathcal{C}_3, \mathcal{C}_4, \mathcal{C}_5) = (0, 0, 0, a_{53}, 0)$

where

$$\begin{aligned}
 a_{21} &= 0.391752226571890, \\
 a_{31} &= 0.217669096261169, & a_{32} &= 0.368410593050371, \\
 a_{41} &= 0.0826920866578107, & a_{42} &= 0.139958502191895, & a_{43} &= 0.251891774271694, \\
 a_{51} &= 0.0679662836371149, & a_{52} &= 0.115034698504631, & a_{53} &= 0.207034898597386, \\
 a_{54} &= 0.544974750228521, \\
 b_1 &= 0.146811876084787, & b_2 &= 0.248482909444976, & b_3 &= 0.104258830331981. \\
 b_4 &= 0.274438900901351, & b_5 &= 0.226007483236906,
 \end{aligned}$$

are the coefficients coming from the five-stage fourth-order ERK method, and

$$\begin{aligned}
 \tilde{a}_{21} &= a_{21} - \mathcal{C}_1, \\
 \tilde{a}_{31} &= a_{31} + (a_{32} - \tilde{a}_{32}) - \mathcal{C}_2, \\
 \tilde{a}_{32} &= a_{32} + 0.35732150216762254 \mathcal{C}_1 - 1.4960468621714111 \mathcal{C}_2, \\
 \tilde{a}_{41} &= a_{41} + (a_{42} - \tilde{a}_{42}) + (a_{43} - \tilde{a}_{43}) - \mathcal{C}_3, \\
 \tilde{a}_{42} &= a_{42} - 1.1710769982806357 \mathcal{C}_1 + 0.5683454330255046 \mathcal{C}_2 \\
 &\quad - 1.2113329061942606 \mathcal{C}_3 - 1.2320330135900457 (a_{53} - \mathcal{C}_4) \\
 &\quad + 6.103552261439627 \mathcal{C}_5, \\
 \tilde{a}_{43} &= a_{43} - 0.37989814851159776 \mathcal{C}_1 + 0.8235256827462162 (a_{53} - \mathcal{C}_4) \\
 &\quad - 4.079786814017799 \mathcal{C}_5, \\
 \tilde{a}_{51} &= a_{51} + (a_{52} - \tilde{a}_{52}) + (a_{53} - \mathcal{C}_4) + (a_{54} - \tilde{a}_{54}) - \mathcal{C}_5, \\
 \tilde{a}_{52} &= a_{52} + 0.1577481084030307 \mathcal{C}_1 + 1.4709109036585493 \mathcal{C}_3 \\
 &\quad + 1.4960468621714111 (a_{53} - \mathcal{C}_4) - 4.121723862609585 \mathcal{C}_5, \\
 \tilde{a}_{54} &= a_{54} - 1.2142912127103236 \mathcal{C}_3 + 1.432293346906654 \mathcal{C}_5.
 \end{aligned}$$

These coefficients are directly those appearing in the corresponding Butcher's tableau (see table 5). Note that in this case, as for the third-order PIRK method, the resulting IMEX-RK has only 5 stages because $b_6 = 0$, and the tableau could be simplified by removing the first stage. For completeness we give the values

of c_i :

$$\begin{aligned} c_1 &= 0, & c_2 &= 0.391752226571890, & c_3 &= 0.58607968931154, \\ c_4 &= 0.4745423631214, & c_5 &= 0.935010630967653, & c_6 &= 1. \end{aligned}$$

We can derive the expression for the matrix M_4 and its determinant, but we prefer to omit them in the text due to their long length. The determinant of the matrix results in a polynomial expression for $(\lambda\alpha_2)$ of degree 5 with coefficients depending on dex , trex , a_{ij} and \tilde{a}_{ij} ; the coefficient for $(\lambda\alpha_2)^5$ only depends on a_{ij} and \tilde{a}_{ij} .

We can now study numerically the behaviour of $\det(M_5)$ for $\omega_i = 0, \pm 1$, $i = 1, 2$, starting from $(\lambda\alpha_2) = 0$ and decreasing this value. Since the determinant is one scalar quantity, in contrast with the more complex analysis for the eigenvalues of M_5 , the numerical study is much easier and very efficient. We start by setting $(\lambda\alpha_2) = -\epsilon$, with ϵ a positive value very close to 0; we then minimize numerically the maximum value of $|\det(M_5)|$ for $\omega_i = 0, \pm 1$, $i = 1, 2$, checking that it stays below 1; with the resulting values for the coefficients \mathcal{C}_i , we plot $|\det(M_5)|$ for $\omega_i = 0, \pm 1$, $i = 1, 2$, and control that $|\det(M_5)| < 1 \quad \forall x \in [-\epsilon, 0]$ for $\omega_i = 0, \pm 1$, $i = 1, 2$; we finally replace ϵ by a greater value and repeat the process until $|\det(M_5)|$ for $\omega_i = 0, \pm 1$, $i = 1, 2$, does not stay below 1 $\forall x \in [-\epsilon, 0]$.

The final values for the coefficients, which satisfy that $|\det(M_5)| < 1 \quad \forall x \in [-27, 0]$ for $\omega_i = 0, \pm 1$, $i = 1, 2$, are:

$$\begin{aligned} \mathcal{C}_1 &= 0.13761208339219633, \quad \mathcal{C}_2 = 0.2042433556378285, \quad \mathcal{C}_3 = 0.0904666765339173, \\ \mathcal{C}_4 &= 0.3966145239174311, \quad \mathcal{C}_5 = -0.00984245655482246. \end{aligned}$$

We call PIRK4 hereafter the PIRK method with these coefficients. For comparison, the optimal five-stage fourth-order ERK method satisfies that $|\det(M_5)| < 1 \quad \forall x \in [-6.75, 0]$ for $\omega_i = 0, \pm 1$, $i = 1, 2$, but $\exists \omega_i = 0, \pm 1$, $i = 1, 2$ such that $|\det(M_5)| > 1$ for $x = -7$.

4.7. Relation between the PIRK methods and the IMEX RK methods

As we mentioned in Sect. 3, s -stages PIRK methods are related to $s + 1$ -stages IMEX ones. Therefore, it seems natural to compare the PIRK methods derived in the previous sections with IMEX RK ones of second, third and fourth-orders existing in the literature. The relation between PIRK1 and the IMEX- θ method has already discussed in Sect. 4.3.

The IMEX-SSP2(2,2,2) method presented in [5] is a three-stages second-order scheme, that particularized to the system (9) reads:

$$\begin{cases} u^{(1)} = u^n, \\ v^{(1)} = v^n + \Delta t L_2(u^n), \end{cases} \quad (72)$$

$$\begin{cases} u^{(2)} = u^n + \Delta t L_1(u^{(1)}, v^{(1)}), \\ v^{(2)} = v^n + \Delta t \left[(1 - 2\gamma)L_2(u^n) + \gamma L_2(u^{(2)}) + L_3(u^{(1)}, v^{(1)}) \right], \end{cases} \quad (73)$$

$$\begin{cases} u^{n+1} = u^n + 0.5\Delta t \left[L_1(u^{(1)}, v^{(1)}) + L_1(u^{(2)}, v^{(2)}) \right], \\ v^{n+1} = v^n + 0.5\Delta t \left[L_2(u^n) + L_2(u^{(2)}) + L_3(u^{(1)}, v^{(1)}) + L_3(u^{(2)}, v^{(2)}) \right], \end{cases} \quad (74)$$

where $\gamma = 1 - 1/\sqrt{2}$. This IMEX method is L-stable regarding the implicit part. In comparison with the second-order PIRK methods (PIRK2a and PIRK2b), there is an additional intermediate stage, which in principle implies additional computations. However, in practice it is only necessary to compute each of the differential operators twice per iteration, albeit at different stage levels (at (1) and (2) for L_1 and L_3 ; at n and (2) for L_2). This effectively transforms the method in a two-stage one (from the point of view of the computation of the differential operators), when applied to systems of separable wave-like equations. Although a smart implementation of this IMEX could in principle give similar computational performance per iteration as the PIRK2 scheme, the complexity added by the three stages of this IMEX scheme (but

only two evaluations of the differential operators) makes it difficult to implement efficiently in existing high performance codes. We think that this is a good reason to make the PIRK2 methods preferable over IMEX ones for the case of separable wave-like equations.

The IMEX-SSP3(4,3,3) method presented in [5] is a five-stages third-order scheme, that particularized to the system (9) reads:

$$\begin{cases} u^{(1)} = u^n, \\ v^{(1)} = v^n + \Delta t L_2(u^n), \end{cases} \quad (75)$$

$$\begin{cases} u^{(2)} = u^n, \\ v^{(2)} = v^n, \end{cases} \quad (76)$$

$$\begin{cases} u^{(3)} = u^n + \Delta t L_1(u^n, v^n), \\ v^{(3)} = v^n + \Delta t \left[(1 - \alpha) L_2(u^n) + \alpha L_2(u^{(3)}) + L_3(u^n, v^n) \right], \end{cases} \quad (77)$$

$$\begin{cases} u^{(4)} = u^n + 0.25 \Delta t \left[L_1(u^n, v^n) + L_1(u^{(3)}, v^{(3)}) \right], \\ v^{(4)} = v^n + \Delta t \left[\beta L_2(u^n) + (0.5 - \alpha - \beta) L_2(u^{(3)}) + \alpha L_2(u^{(4)}) \right. \\ \left. + 0.25 L_3(u^n, v^n) + 0.25 L_3(u^{(3)}, v^{(3)}) \right], \end{cases} \quad (78)$$

$$\begin{cases} u^{n+1} = u^n + \frac{\Delta t}{6} \left[L_1(u^n, v^n) + L_1(u^{(3)}, v^{(3)}) + 4L_1(u^{(4)}, v^{(4)}) \right], \\ v^{n+1} = v^n + \frac{\Delta t}{6} \left[L_2(u^n) + L_2(u^{(3)}) + 4L_2(u^{(4)}) \right. \\ \left. + L_3(u^n, v^n) + L_3(u^{(3)}, v^{(3)}) + 4L_3(u^{(4)}, v^{(4)}) \right], \end{cases} \quad (79)$$

where $\alpha = 0.24169426078821$, $\beta = 0.18957643480295$. Due to the particular structure of the system (9), the resulting two first stages can be omitted, and the effective number of stages is the same as in the case of third-order PIRK methods. The trivial value for $v^{(2)}$ results from a cancellation, as a consequence of the presence of opposite coefficients in the second stage of the numerical scheme. Actually, for this system of equations, the IMEX-SSP3(4,3,3) method corresponds to a third-order PIRK one, with $\mathcal{C}_1 = \alpha = 0.24169426078821$ and $\mathcal{C}_2 = (1 - 3\mathcal{C}_1)/4 = 0.06872930440884$ (see also table 4). These values for the \mathcal{C}_i coefficients are close to one of the optimal sets deduced in Sect. 4.5, $\mathcal{C}_1 = 4\mathcal{C}_2 = 1/4$. As expected, both schemes will perform in a very similar way in the numerical examples shown in the next sections.

As we have shown in the previous section, the derivation of the fourth-order PIRK method is relatively simple, due to the fact that it is based on the analysis of a scalar quantity. On the contrary, the derivation of high-order IMEX methods when we do not focus on a particular structure of equations is quite complex; for example, Kennedy and Carpenter derived several schemes up to fifth-order of convergence in [31].

5. Application 1: system of ODEs

Let us consider a system of ODEs of the following form:

$$u_t = c u + d v, \quad v_t = a u + b v, \quad (80)$$

where a , b , c and d are real constants. This system is interesting because it coincides with the linear part of the system of equations (10) considered for our stability analysis, with $\bar{\alpha}_1 = c$, $\bar{\alpha}_2 = d$, $\bar{\gamma}_1 = 0$, $\bar{\gamma}_2 = b$ and $\bar{\lambda} = a$.

In the case $(b - c)^2 + 4 a d < 0$ and $b + c \leq 0$, this system of equations has damped oscillatory solutions of the form,

$$u = \frac{\sqrt{-ad}}{a} v_0 \cos(\omega t + \phi) e^{\sigma t}, \quad v = v_0 \cos(\omega t) e^{\sigma t}, \quad (81)$$

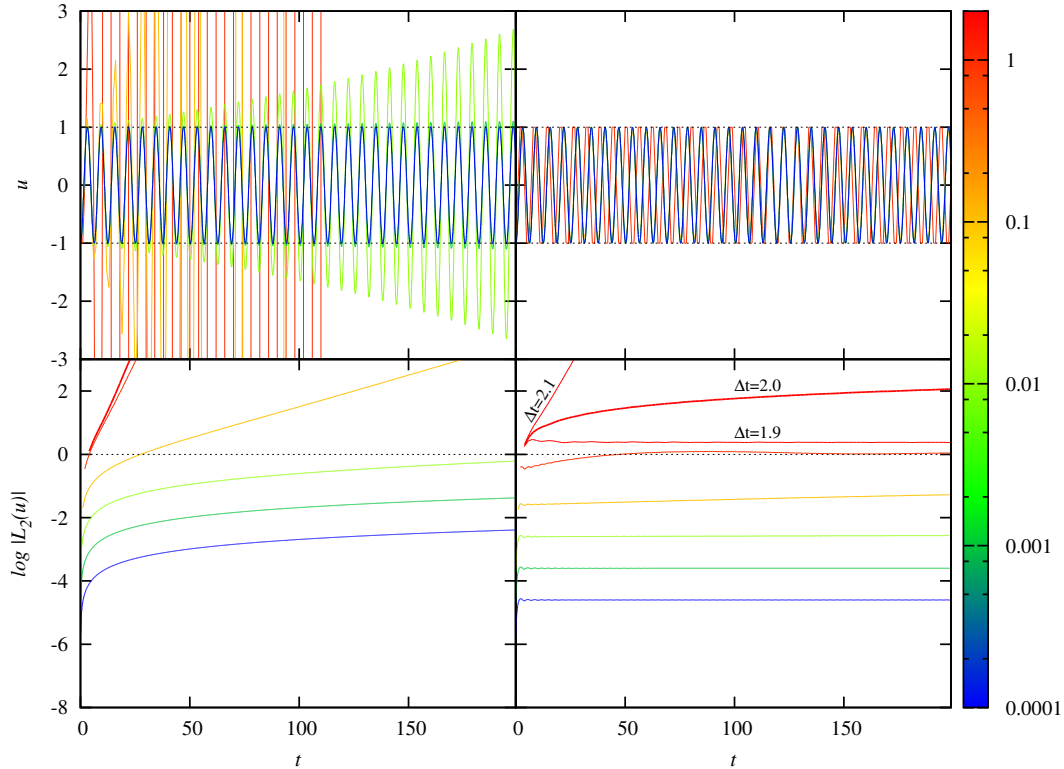


Figure 1: Numerical integration of a system of ODEs with $\sigma = \phi = 0$ and $\phi = \pi/2$, using a first-order ERK method (left panels) and a first-order PIRK method (right panels). Upper panels show the time evolution of u , for $10^{-4} \leq \Delta t \leq 1$. Dotted lines are the amplitude of the oscillatory analytic solution. Lower panels show the time averaged L_2 -norm of the difference between the numerical and analytical solutions, for $10^{-4} \leq \Delta t \leq 2.1$. Different lines are colored according to the time step, Δt , used in each simulation.

being v_0 , $\omega \equiv \frac{1}{2}\sqrt{-4ad - (b-c)^2}$, $\sigma \equiv \frac{b+c}{2}$ and $\tan \phi \equiv \frac{\omega}{\sigma-b}$ a constant set by the initial conditions, the frequency, decay rate and relative phase between u and v , respectively. This system corresponds to (9), with $\mathcal{L}_1(u, v) = u + v$, $\mathcal{L}_2(u) = au$ and $\mathcal{L}_3(u, v) = bv$. Depending on the values of ω , σ and ϕ , the applicability requirements of the PIRK methods given by definition (2.2) may impose restrictions over the possible values of Δt that can be used: $\bar{\alpha}_2 \bar{\lambda} < 0$ is fulfilled always; $|\text{trex}| \leq 2 \Leftrightarrow \Delta t \leq -2/\sigma$; and $|\text{dex}| \leq 1 \Leftrightarrow -2/\Delta t \leq 2\sigma + (\sigma^2 - \omega^2 \cot^2 \phi)\Delta t \leq 0$. We comment here which restrictions result for the cases considered in the numerical simulations carried out in this section. For $\sigma = 0$ and $\phi = \pi/2$, we have no restriction for the time-step, $\Delta t < \infty$. For $\sigma < 0$ and $\phi = \pi/2$, then $\Delta t < -2/\sigma$. For $\sigma = 0$ and $0 < \phi < \pi/2$, then $\Delta t < \frac{\sqrt{2} \tan \phi}{\omega}$.

For our numerical experiment we will consider the case $\omega = 1$ and $a = -d$, without loss of generality, since it is equivalent to a rescaling of t and v . The remaining coefficients depend only on the values of σ and ϕ . We have performed numerical simulations for $\sigma = 0, -0.01, -0.1, -1$, and $\phi/\pi = 1/2, 1/3, 1/4, 1/10$, which are representative of all possible solutions of this set of equations. As initial condition we use the analytical values of u and v , given by Eq. (81), at $t = 0$, and $v_0 = 1$.

Fig. 1 shows the results for a representative test, comparing the first-order ERK method with the first-order PIRK method. To estimate the relative error of the method we compute the time-averaged L_2 -norm

of the difference between the analytic and the numerical solutions:

$$L_2(u)(t) = \frac{1}{t} \sqrt{\sum_{t_n < t} [u_{\text{num}}(t_n) - u_{\text{ana}}(t_n)]^2 \Delta t^2 e^{-2\sigma t_n}} . \quad (82)$$

For this test the ERK method is unconditionally unstable (see left panels) and decreasing the time step leads to an exponentially increasing amplitude, provided the integration time is sufficiently long. By comparison, the first-order PIRK method is stable for $\Delta t < 2$, since $|u| \lesssim 1$. Using the PIRK method, the solution loses accuracy at late times (in this case a phase shift), but it is still bounded (e.g. for $\Delta t = 0.1$ at $t = 1000$), and hence the numerical method is stable.

We use the value of the time-averaged L_2 -norm at time $t = 100$ as a measure of the stability of a numerical method, for a particular numerical test with a given time step. Values < 1 (> 1) usually indicate stability (instability). In Fig. 2 we compare the stability properties of the ERK and PIRK methods, for different orders of convergence, observed in our numerical experiments when $\sigma = 0$ and $\phi = \pi/2$. In all cases, the PIRK methods are superior to the ERK methods, as they can achieve stable numerical evolutions with significantly longer time steps. For small time steps, all numerical methods follow the expected order of convergence. For first and second-order methods, ERK methods are unconditionally unstable; despite L_2 -norm < 1 for small values of Δt , longer evolutions always lead to exponentially growing amplitudes in all studied cases. In contrast, first and second-order PIRKs are numerically stable in all simulations tested (up to $t = 1000$), and only become unstable for Δt larger than a certain threshold. For the third and fourth-order methods, all the schemes are stable for small Δt , but the ERK schemes become unstable at lower values of Δt than the PIRK ones; the third-order PIRK methods behave similar to the tested IMEX scheme.

A change of the value of σ , fixed $\phi = \pi/2$, introduces a damping in the oscillatory solution, in a timescale of $1/\sigma$. As the parameters approach $|\sigma\omega| \sim 1$, the system becomes stiff, and the maximum time-step providing stable evolutions decreases as expected. Presenting as an example the case of third-order methods (see upper panel of Fig. 3), and similarly for first, second and fourth-order ones, as we approach $\sigma = -1$, both the ERK and PIRK methods behave almost identically. Despite of the PIRK method being *partially implicit*, the terms in Eq. (80) responsible for the stiffness cannot be included in the \mathcal{L}_2 operator, and both the ERK and PIRK methods suffer from this stiffness problem.

In the case of varying ϕ , fixed $\sigma = 0$, all the ERK schemes behave in an identical way (see lower-right panel of Fig. 3 for third-order schemes; first, second and fourth-order ones behave similarly). However, the PIRK methods suffer from a significant reduction of the maximum time step as $\phi \approx \pi/2$ (see lower-middle and right panels of Fig. 3 for third-order schemes; first, second and fourth-order ones behave similarly). This is the only case in which the ERK methods are superior to the PIRK methods. Therefore, the class of systems for which the PIRK methods are a good alternative to the classical ERK methods are wave-like equations, in which the condition $\phi \approx \pi/2$ is fulfilled.

6. Application 2: Scalar wave equation

Our second test case is the time evolution of a scalar wave equation in spherical coordinates. Our motivation for choosing this test is the difficulties that the numerical relativity community has traditionally encounter evolving Einstein equations in these particular set of coordinates. The case of Einstein equations involves the evolution of non-linear wave-like equations for tensorial quantities. To elude the difficulties of evolving such systems of equations and have a clean test of our numerical methods with analytic exact solutions, we have chosen here to study the evolution of an scalar wave equation. Therefore, we have concentrated most of our effort in this particular test, for which the most detailed analysis is given here. The wave equation in Cartesian coordinates is also studied, at the end of this section, albeit less thoughtfully, to check that the stability properties of the system of equations do not depend on the system of coordinates (as it should be from the analysis carried out in Sect. 4).

A wave equation for a scalar h can be written as:

$$\partial_{tt}h = \Delta h, \quad (83)$$

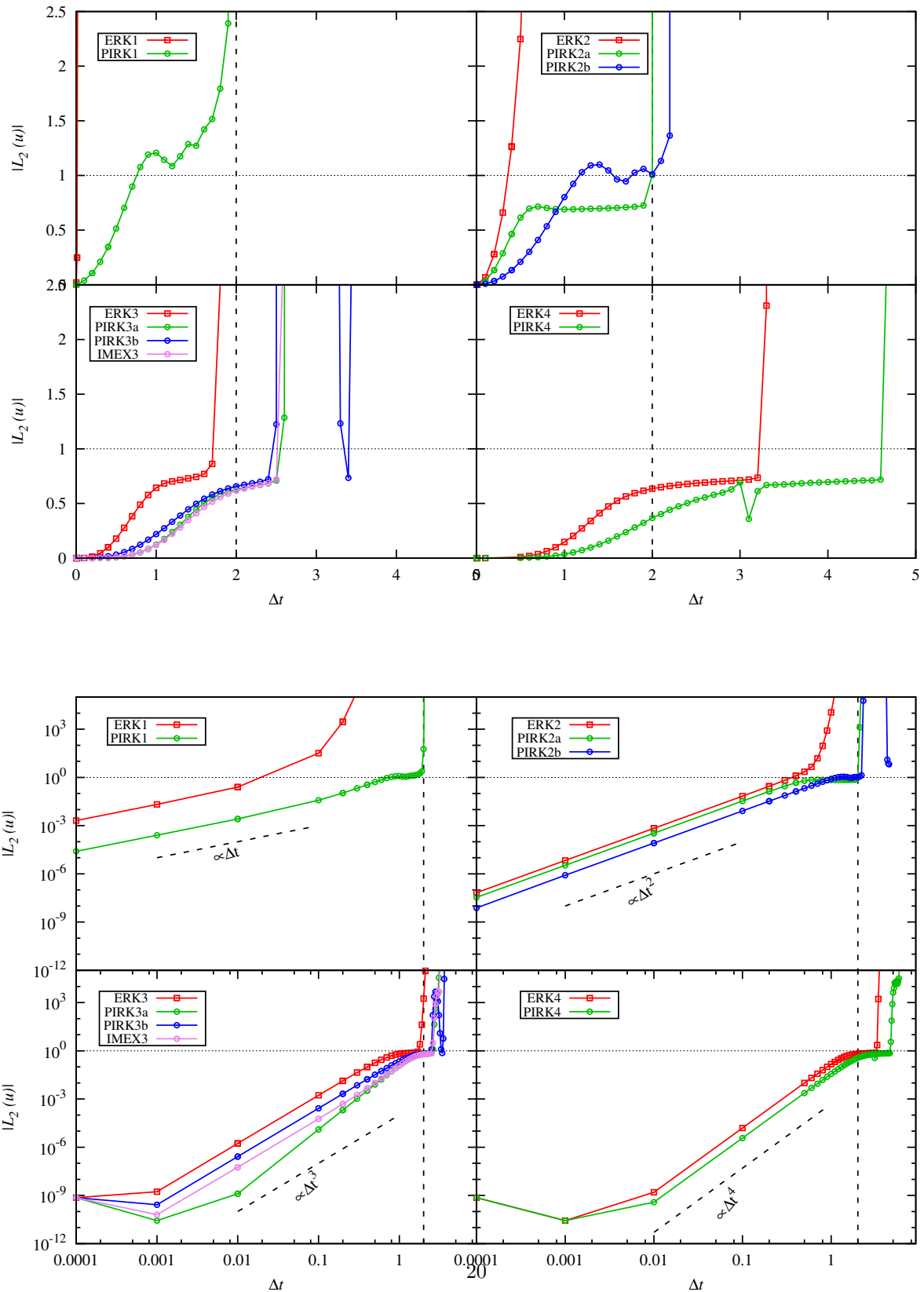


Figure 2: Numerical error integrating a system of ODEs with $\sigma = 0$ and $\phi = \pi/2$, using first, second, third and fourth-order methods. Upper panels show the transition between stable ($L_2 \ll 1$) and unstable ($L_2 \gg 1$) numerical evolutions. Lower panels, in logarithmic scale, show the behavior for small time steps, compared to the expected scaling for each method (dashed-dotted lines). As a reference, vertical dashed line at $\Delta t = 2$ corresponds to the maximum time step for the first-order PIRK method to be stable.

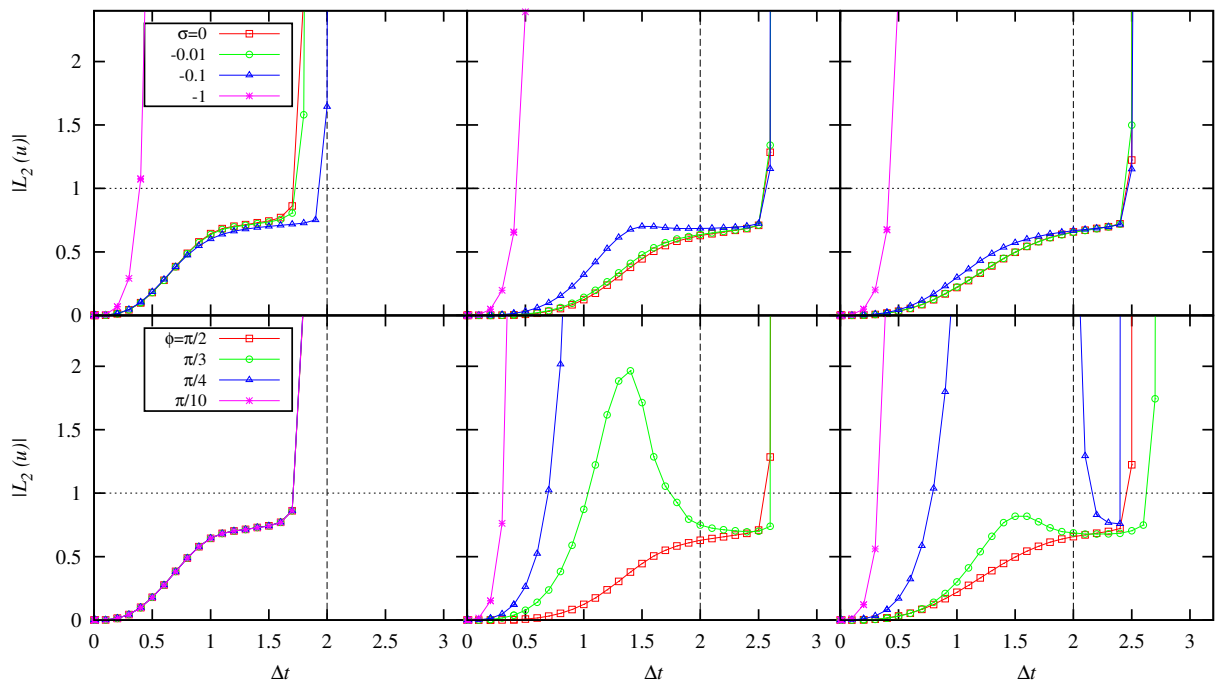


Figure 3: Behavior of the error for third-order schemes for different values of σ (upper panels, $\phi = \pi/2$) and ϕ (lower panels, $\sigma = 0$). From left to right, third-order ERK, PIRK3a and PIRK3b schemes.

where Δ is the Laplacian operator. Eq. (83) can be rewritten as a first-order system in time, with the addition of an extra auxiliary variable, A , as follows:

$$\begin{aligned}\partial_t h &= A, \\ \partial_t A &= \Delta h.\end{aligned}\tag{84}$$

In this case, according to system (9), the variables can be identified as $(u, v) = (h, A)$, and the operators as $\mathcal{L}_1(h, A) = A$, $\mathcal{L}_2(h) = \Delta h$ and $\mathcal{L}_3(h, A) = 0$. Therefore, $\bar{\alpha}_1 = \bar{\gamma}_1 = \bar{\gamma}_2 = 0$ and $\bar{\alpha}_2 = 1$ in system (10). The eigenvalues of the linearized explicit part are $\omega_1 = \omega_2 = 1$ and hence $\text{dex} = 1$ and $\text{trex} = 2$. $\bar{\lambda} \in \mathbb{R}^-$ and its value depends on the particular solution for h and the discretization of the operator Δ . Spherical coordinates are used, being $\left(\frac{\partial}{\partial r}, \frac{1}{r} \frac{\partial}{\partial \theta}, \frac{1}{r \sin \theta} \frac{\partial}{\partial \varphi}\right)$ the corresponding orthonormal basis.

Eq. (83) has solutions of the form

$$h(r, \theta, \varphi, t) \sim j_l(kr) Y_{lm}(\theta, \varphi) \cos kt,\tag{85}$$

being j_l the spherical Bessel function of first kind of order l and Y_{lm} the spherical harmonics. The value of k , a positive real constant, is determined by imposing boundary conditions. We search for solutions inside a sphere of radius unity imposing $h(r = 1, \theta, \varphi, t) = 0$. For fixed l and m , it is possible to compute the eigenmode frequencies, k_{nl} , as the zeros of the spherical Bessel function of order l , being $n = 1$ the first zero and so on.

We have performed 1D-spherical, 2D-axisymmetric and 3D simulations of the system using as initial data solutions with $n = 1$ at $t = 0$. We use values of $(l, m) = (0, 0), (2, 0), (2, 2)$, for the 1D, 2D and 3D case, respectively. In this way, the initial data are regular and fulfill the symmetries in each case. Furthermore, the data are non trivial for each symmetry, in the sense that there are not trivial cancellations for 2D and 3D simulations. We consider symmetry with respect to the equatorial plane, $\theta = \pi/2$.

We use a finite difference scheme to solve the system using an equally-spaced grid with n_r, n_θ and n_φ grid points in the r, θ and φ directions, respectively. We use derivatives of cell-centered Lagrange interpolation polynomials [33] to compute the first and second spatial derivatives appearing in the Laplacian operator, achieving fourth, sixth and eighth discretization order. Boundary conditions are imposed by using a number of ghost cells consistent with the discretization stencil. The analytical solution is imposed as boundary condition at $r = 1$. Symmetry conditions are used at all other boundaries. The maximum time step is determined by the CFL condition for the speed of the wave, which is 1. The time step in the simulations is a smaller fraction of the maximum time step, the CFL factor, in the interval $[0, 1]$.

We can estimate the absolute error of the numerical evolution by comparing the numerical solution with the analytical one given by Eq. (85). As a measure of the global error during the numerical evolution, we compute the L_2 -norm of the difference between the numerical and the analytical solutions at a given time,

$$L_2(h)(t) = \frac{1}{n_r n_\theta n_\varphi} \sqrt{\sum_{r, \theta, \varphi} [h_{\text{num}}(r, \theta, \varphi, t) - h_{\text{ana}}(r, \theta, \varphi, t)]^2 (kr)^2}.\tag{86}$$

6.1. Stability

We have studied numerically the stability of the first, second and third-order PIRK methods. This study involves the numerical computation of a wide parameter space, including the coefficients \mathcal{C}_i of the PIRK methods and the CFL factor. Up to 10000 simulations have to be performed to cover this parameter space, so we have decided to use a single numerical setup as reference for the stability study. We use $(n, l, m) = (1, 2, 0)$ for the initial data in 2D-axisymmetry with equatorial symmetry. In this case, $k_{12} \approx 5.763$. We use $(n_r, n_\theta) = (100, 32)$ grid points and a fourth-order spatial discretization scheme.

With the numerical setup fixed, we can estimate the value of $x := -\lambda \alpha_2 = -\bar{\lambda}(\Delta t)^2$, which is the relevant quantity for the stability of the system. For solutions of the form (85), Eq. (84) can be written as

$$\begin{aligned}\partial_t h &= A, \\ \partial_t A &= -k^2 h.\end{aligned}\tag{87}$$

Therefore, $\bar{\lambda} = -k^2$. The minimum value of k corresponds to the fundamental mode $(n, l, m) = (1, 0, 0)$, i.e. $k_{\min} = k_{10} = \pi$. This sets the lower limit for x ,

$$x_{\min} = \pi^2(\Delta t)^2. \quad (88)$$

Note that in the limit of infinite resolution, the CFL restriction results in $\Delta t \rightarrow 0$ and $x_{\min} \rightarrow 0$. We show in the next subsections that this is indeed the case for the typical resolutions used in practical applications.

The maximum value of k corresponds to solutions with typical spatial variations of the order of the smallest grid cell size, Δl_{\min} . For these solutions,

$$k_{\max} \approx \frac{2\pi}{\Delta l_{\min}}, \quad (89)$$

and hence the upper limit for x is

$$x_{\max} = k_{\max}^2(\Delta t)^2 \approx \left(\frac{2\pi\Delta t_{\max}}{\Delta l_{\min}}\right)^2 (\text{CFL factor})^2 = 4\pi^2(\text{CFL factor})^2, \quad (90)$$

being the CFL factor $= \Delta t/\Delta t_{\max}$ and $\Delta t_{\max} = \Delta l_{\min}$ the maximum time step allowed by the CFL condition, which coincides with the smallest grid cell size. Note that x_{\max} does not depend on the resolution. As a consequence, the stability properties of the system do not depend on the resolution, but only on the CFL factor. For convenience we define $\bar{x} := x/(\text{CFL factor})^2$; therefore, $\bar{x}_{\min} = \pi^2(\Delta t_{\max})^2$ and $\bar{x}_{\max} = 4\pi^2$. By keeping the numerical setup fixed, we expect that the limits of \bar{x} stay constant in all our simulations. Effects of the dimensionality and resolution are discussed in Sect. 8.

For each order of the PIRK methods, we compare stability behavior of the numerical simulations with the stability criterion of Sect. 4 for the determinant of the corresponding matrix of a given method. We compare this stability criterion with the general one for the eigenvalues of the system.

6.1.1. First-order method

The expression for $\det(M_1)$ particularized to the system (84) with $x > 0$, is

$$\det M_1 = 1 + (1 - \mathcal{C}_1)x, \quad (91)$$

and the eigenvalues of M_1 are

$$e_{\pm} = \frac{1}{2} \left(2 - \mathcal{C}_1 x \pm \sqrt{-x(4 - \mathcal{C}_1^2 x)} \right). \quad (92)$$

The stability criterion, $|e_{\pm}| \leq 1$, for $x \neq 0$, results in

$$1 \leq \mathcal{C}_1 \leq \frac{1}{2} + \frac{2}{x}, \quad (93)$$

$$x \leq 4. \quad (94)$$

The condition $|\det M_1| \leq 1$, used in Sect. 4, results in

$$1 \leq \mathcal{C}_1 \leq 1 + \frac{2}{x}, \quad (95)$$

which is a necessary, but not sufficient, condition for stability. Conditions (93)–(95) are more restrictive for larger values of x , so the value \bar{x}_{\max} determines the stability properties of the system.

It is therefore relevant to study the stability properties of the numerical solution depending on the coefficient \mathcal{C}_1 and the time step Δt . We have performed series of simulations for several CFL factors (0.3, 0.4, 0.5, 0.6, 0.7, 0.8, 0.85 and 0.9), varying the value of \mathcal{C}_1 from 0 to 5 in steps of 0.001 (4×10^4 simulations in total). We have evolved each simulation up to time $t = 54$, i.e. about 50 oscillations. The left panel of Fig. 4 shows the evolution of the L_2 -norm for a selection of simulations. The behavior of this quantity allows

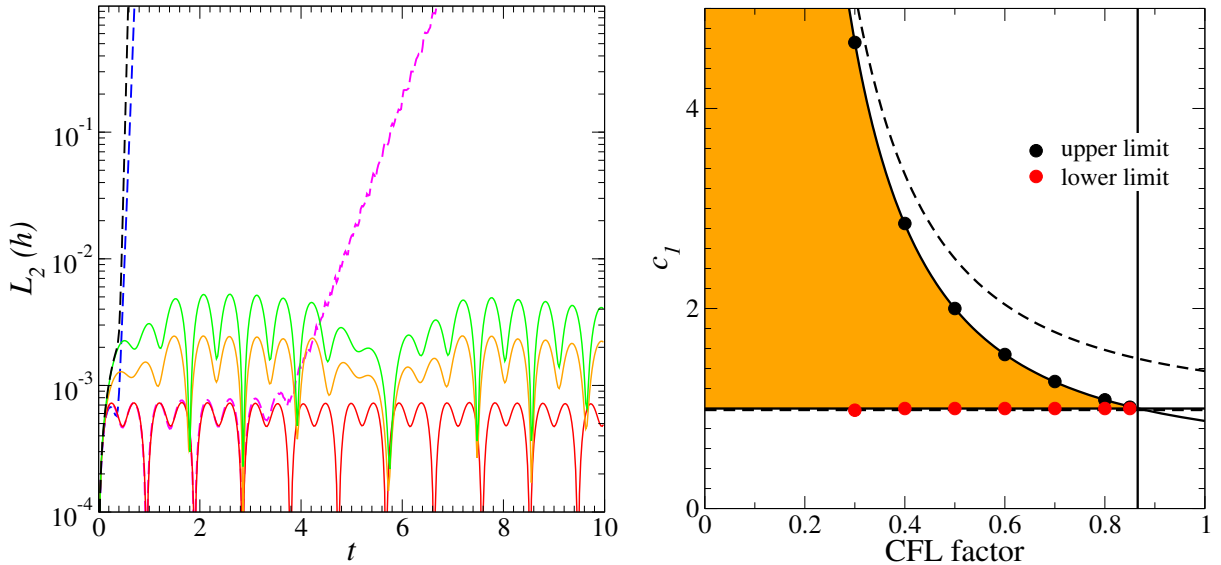


Figure 4: Stability of the first-order PIRK method. *Left panel:* time evolution of the L_2 -norm for simulations with CFL factor 0.5 and C_1 values of 0.9 (blue), 0.99 (magenta), 1 (red), 1.5 (orange), 2 (green) and 2.05 (black). Solid and dashed lines represent numerically stable and unstable simulations, respectively. *Right panel:* stability region depending on the values for C_1 and the CFL factor. Red and black circles are the maximum and minimum values of C_1 , respectively, for which a numerically stable evolution is found for each CFL factor. Solid lines are the boundaries of the stability region (orange area) given by Eqs. (93) and (94), for the fitted value of $\bar{x} = 5.340$. The boundary of the region $|\det(M_1)| \leq 1$, which partially coincides with the stability boundaries, is also plotted (dashed lines).

us to distinguish between numerically stable and unstable evolutions in a similar fashion as we did for the ODE case of Sect. 5. Numerically stable evolutions (solid lines) show an oscillatory behavior of the L_2 -norm with values smaller than one, while numerically unstable evolutions (dashed lines) show an exponential growth of the L_2 -norm which becomes much larger than 1. For the purpose of this test, we consider a numerical simulation to be numerically stable at a point of the parameter space, given by the CFL factor and the coefficients of the PIRK method, if L_2 -norm < 1 at a time corresponding to 50 oscillations, i.e. $t = 100\pi/\omega$.

For each CFL factor, we find a maximum and minimum values of C_1 such that all simulations within this two values are numerically stable, while lower or higher values lead to numerically unstable evolutions. No numerically stable values of C_1 were found for a CFL = 0.9. The right panel of Fig. 4 shows the numerically determined stability limits (red and black circles). We can compare these limits with the predictions of Eqs. (93) and (94). For all CFL factors the lower limit is $C_1 = 1$ and coincides with the prediction of Eq. (93). Following Eq. (93), we fit the upper bound by a curve of the form $p_1 + p_2(\Delta t_{\max}/\Delta t)^2$, with $p_1 = 0.501$, $p_2 = 0.3746$ and Δt_{\max} the maximum time step predicted by the CFL condition. We confirm the $1/(\Delta t)^2$ behavior of the upper limit and a value of p_1 compatible with the predicted $1/2$ in Eq. (93). From the fitted value of p_2 we estimate $\bar{x} = 5.340$, which is of the order of magnitude of $\bar{x}_{\max} \approx \pi^2$. Using this estimation for \bar{x} , it is possible to compute the maximum CFL factor using the condition (94). It results to be 0.8656, consistent with not finding any stable simulation for CFL = 0.9.

If we consider the stability criterion used in Sect. 4.3 (dashed-line in Fig. 4) for the determinant of M_1 , we observe that this criterion is overestimating the stability region. However, the estimated optimal value, $C_1 = 1$, lays inside the stability region and is indeed the value such that the maximum CFL factor is achievable.

The first-order ERK method can be recovered by setting $C_1 = 0$ ¹. Since none of our numerical simulations

¹Alternatively, identical result can be obtained by setting $\bar{\alpha}_1 = \bar{\gamma}_1 = \bar{\lambda} = 0$, $\bar{\alpha}_2 = 1$ and $\bar{\gamma}_1 \neq 0$ for all of the PIRK methods presented in this work.

with $\mathcal{C}_1 = 0$ and CFL factors between 0.3 and 0.95 show stable evolutions (see right panel of Fig. 4), we have performed simulations decreasing the CFL factor to try to find the stability limit. We were not able to find stable evolutions for CFL factors as low as 0.001. The reason for this behavior is that the eigenvalues of the first-order ERK method, given by Eq. (92) with $\mathcal{C}_1 = 0$, read

$$e_{\pm} = 1 \pm \sqrt{-x}, \quad (96)$$

and the stability criterion, $|e_{\pm}| \leq 1$, is only fulfilled for $x = 0$, i.e. $\Delta t = 0$. If we decrease the CFL factor, i.e. approach $|e_{\pm}| = 1$, the instability appears at later time in the simulation (e.g., for CFL = 0.001 the instability appears at $t \sim 7$). The consequence is that first-order ERK method can be used for finite-time evolutions provided a sufficiently small CFL factor is used. However, the time step restriction of the first-order ERK method is significantly larger (several orders of magnitude) than the one of the first-order PIRK scheme.

6.1.2. Second-order method

The expression for $\det(M_2)$ particularized to the system (84) with $x > 0$, is

$$\det(M_2) = \frac{1}{4} [4 - x(2\mathcal{C}_2 - \mathcal{C}_1 - 2\mathcal{C}_1\mathcal{C}_2)], \quad (97)$$

and the eigenvalues of M_2 are

$$\begin{aligned} e_{\pm} &= 1 - \frac{x}{2} + \frac{\mathcal{C}_1}{8}(1 - 2\mathcal{C}_2)x^2 \\ &\pm \frac{1}{8}\sqrt{-x[64 - 16(1 + 2\mathcal{C}_1 - 2\mathcal{C}_2)x + 8\mathcal{C}_1(1 - 2\mathcal{C}_2)x^2 - \mathcal{C}_1^2(1 - 2\mathcal{C}_2)^2x^3]}. \end{aligned} \quad (98)$$

The stability condition, $|e_{\pm}| \leq 1$, leads to

$$\frac{4}{x} \left(1 - \frac{4}{x}\right) \leq \mathcal{C}_1(1 - 2\mathcal{C}_2) \leq \frac{4}{x}, \quad (99)$$

$$\mathcal{C}_1 - \mathcal{C}_2 \leq 2/x, \quad (100)$$

$$\mathcal{C}_2(2\mathcal{C}_1 - 1) \leq \frac{2}{x} \left(-1 + \frac{4}{x}\right), \quad (101)$$

$$0 \leq \mathcal{C}_1 + 2\mathcal{C}_2(\mathcal{C}_1 - 1). \quad (102)$$

The condition $|\det(M_2)| \leq 1$ is equivalent to

$$0 \leq \mathcal{C}_1 + 2\mathcal{C}_2(\mathcal{C}_1 - 1) \leq \frac{8}{x^2}, \quad (103)$$

which coincides partially with the boundaries of the stability region. The conditions (99)-(102) and (103) are more restrictive for larger values of x , therefore the value \bar{x}_{\max} determines the stability properties of the system.

We have studied the numerical stability of the second-order PIRK method by performing simulations using $\mathcal{C}_1 \in [-0.5, 1.5]$ and $\mathcal{C}_2 \in [-0.5, 1.5]$, varying the coefficients in steps of 0.02. We have used several CFL values (0.5, 0.7, 0.8 and 0.9). Fig. 5 shows the stability region on the $(\mathcal{C}_1, \mathcal{C}_2)$ plane. Points of this plane leading to numerically stable simulations are plotted in orange color in Fig. 5, while numerically unstable simulations ($L_2\text{-norm} > 1$ at $t = 100\pi/\omega$) are plotted in white. We use the same convention for the third-order method tests (Fig. 6).

According to Eqs. (99)-(102), the boundaries of the stability region depend only on the parameter \bar{x} . In order to estimate \bar{x} , we perform a χ^2 -minimization of the difference between the numerically determined boundaries for all CFL factors and the theoretically predicted values. We obtain $\bar{x} = 5.373$ with high significance ($\chi^2 = 353.7$ for 385 degrees of freedom). Note that, as expected, the value of \bar{x} is very close

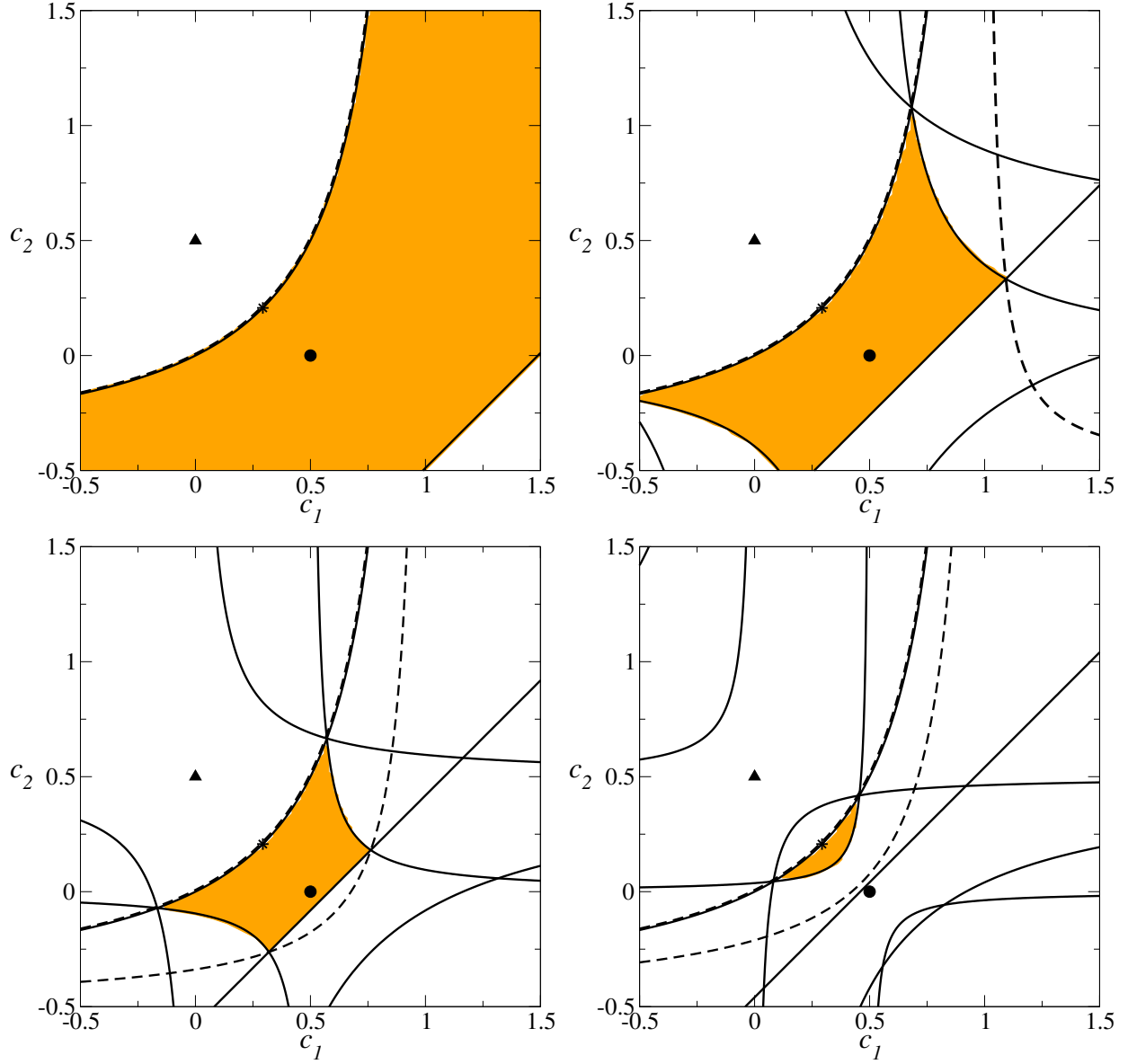


Figure 5: Dependence of the numerically determined stability region (orange area) on the (c_1, c_2) coefficients for the evolution of h using a second-order PIRK method. The boundaries (solid lines) of the stability region according to Eqs. (99)-(102) for $\bar{x} = 5.373$, and the boundaries (dashed lines) of the region $|\det(M_2)| \leq 1$, which partially coincide with the stability boundaries, are plotted. The values for the optimal second-order PIRK method with $(c_1, c_2) = (1/2, 0)$ (PIRK2a, black circle) and $(c_1, c_2) = 1/2(2 - \sqrt{2}, \sqrt{2} - 1)$ (PIRK2b, star symbol), and the second-order ERK scheme (black triangle) are also plotted.

to the one obtained in the first-order PIRK method. The boundaries for the fitted value of \bar{x} (solid-lines in Fig. 5) agree very closely with the numerically computed ones. As in the first-order PIRK method, the criterion $|\det M_2| \leq 1$ overestimates the stability region (dashed-lines in Fig. 5).

We can compare the numerical results for the stability region with the optimal values computed in Sect. 4.4: $(\mathcal{C}_1, \mathcal{C}_2) = (1/2, 0)$ for $|x| \ll 1$ (PIRK2a, black circle in Fig. 5) and $(\mathcal{C}_1, \mathcal{C}_2) = \frac{1}{2}(2 - \sqrt{2}, \sqrt{2} - 1)$ for $|x| \gg 1$ (PIRK2b, star symbol in Fig. 5). Both values allow for stable numerical evolutions with CFL factors close to unity. According to the fit, $x = 5.373$ (CFL factor)², which is larger than unity for CFL factors larger than 0.434. Indeed, the PIRK2b is better suited for higher CFL values, while the PIRK2a becomes unstable. Therefore, we recommend the optimal values $(\mathcal{C}_1, \mathcal{C}_2) = \frac{1}{2}(2 - \sqrt{2}, \sqrt{2} - 1)$ (PIRK2b) as they seem to provide stable evolutions with the largest possible CFL factors.

The second-order ERK scheme corresponds to the case $(\mathcal{C}_1, \mathcal{C}_2) = (0, 1/2)$ and is unconditionally unstable. In this case, the eigenvalues are

$$e_{\pm} = 1 - \frac{x}{2} \pm \sqrt{-x}, \quad (104)$$

and the stability criterion, $|e_{\pm}| \leq 1$, is only fulfilled for $\Delta t = 0$. Therefore, the observed numerical behavior of the second-order ERK scheme is very similar to the first-order ERK one.

6.1.3. Third-order method

The expression for $\det(M_3)$ particularized to the system (84) with $x > 0$ is

$$\det(M_3) = 1 + \frac{x^2}{12}(\mathcal{C}_1 - 4\mathcal{C}_2) + \frac{x^3}{72}[-1 + 3(1 - 2\mathcal{C}_1)(\mathcal{C}_1 + 4\mathcal{C}_2)], \quad (105)$$

and the eigenvalues of M_3 are

$$e_{\pm} = 1 - \frac{x}{2} + \frac{x^2}{24}(1 + \mathcal{C}_1 - 4\mathcal{C}_2) - \frac{\sqrt{x}}{24} [192(x - 3) - 16x^2(3\mathcal{C}_1(1 - \mathcal{C}_1 - 4\mathcal{C}_2) + 1) + x^3(1 + \mathcal{C}_1 - 4\mathcal{C}_2)^2]^{1/2}. \quad (106)$$

The stability criterion, $|e_{\pm}| \leq 1$, for $x \neq 0$ results in

$$\frac{12}{x} \left(1 - \frac{4}{x}\right) \leq 1 + \mathcal{C}_1 - 4\mathcal{C}_2 \leq \frac{12}{x}, \quad (107)$$

$$1 + 3(2\mathcal{C}_1 - 1)(\mathcal{C}_1 + 4\mathcal{C}_2) \leq \frac{6}{x} \left(\frac{12}{x} - 1\right), \quad (108)$$

$$1 + 3(2\mathcal{C}_1 - 1)(\mathcal{C}_1 + 4\mathcal{C}_2) \leq \frac{6}{x} \left[\frac{12}{x} \left(\frac{4}{x} - 1\right) - 1 + 2(1 + \mathcal{C}_1 - 4\mathcal{C}_2) \right], \quad (109)$$

$$\frac{6}{x}(\mathcal{C}_1 - 4\mathcal{C}_2) \leq 1 + 3(2\mathcal{C}_1 - 1)(\mathcal{C}_1 + 4\mathcal{C}_2). \quad (110)$$

The condition $|\det(M_3)| \leq 1$ is equivalent to

$$\frac{6}{x}(\mathcal{C}_1 - 4\mathcal{C}_2) \leq 1 + 3(2\mathcal{C}_1 - 1)(\mathcal{C}_1 + 4\mathcal{C}_2), \quad (111)$$

$$-144 \leq 6x^2(\mathcal{C}_1 - 4\mathcal{C}_2) + x^3[-1 + 3(1 - 2\mathcal{C}_1)(\mathcal{C}_1 + 4\mathcal{C}_2)], \quad (112)$$

which coincides partially with the boundaries of the stability region. The conditions (107)-(109) and (112) are more restrictive for larger values of x , therefore the value \bar{x}_{\max} determines the stability properties of the system at these boundaries. However the condition (110) (which is equivalent to (111)), can be more restrictive for small values of x depending on the value of \mathcal{C}_1 and \mathcal{C}_2 . For this case, both \bar{x}_{\max} and \bar{x}_{\min} are relevant for the stability analysis.

We have performed the same numerical stability analysis for the third-order PIRK method as in Sect. 6.1.2. The numerically computed stability regions depending on $(\mathcal{C}_1, \mathcal{C}_2)$ are shown in Fig. 6 for different CFL factors. As in the second-order method, the stability regions shrinks for increasing CFL factors. We have

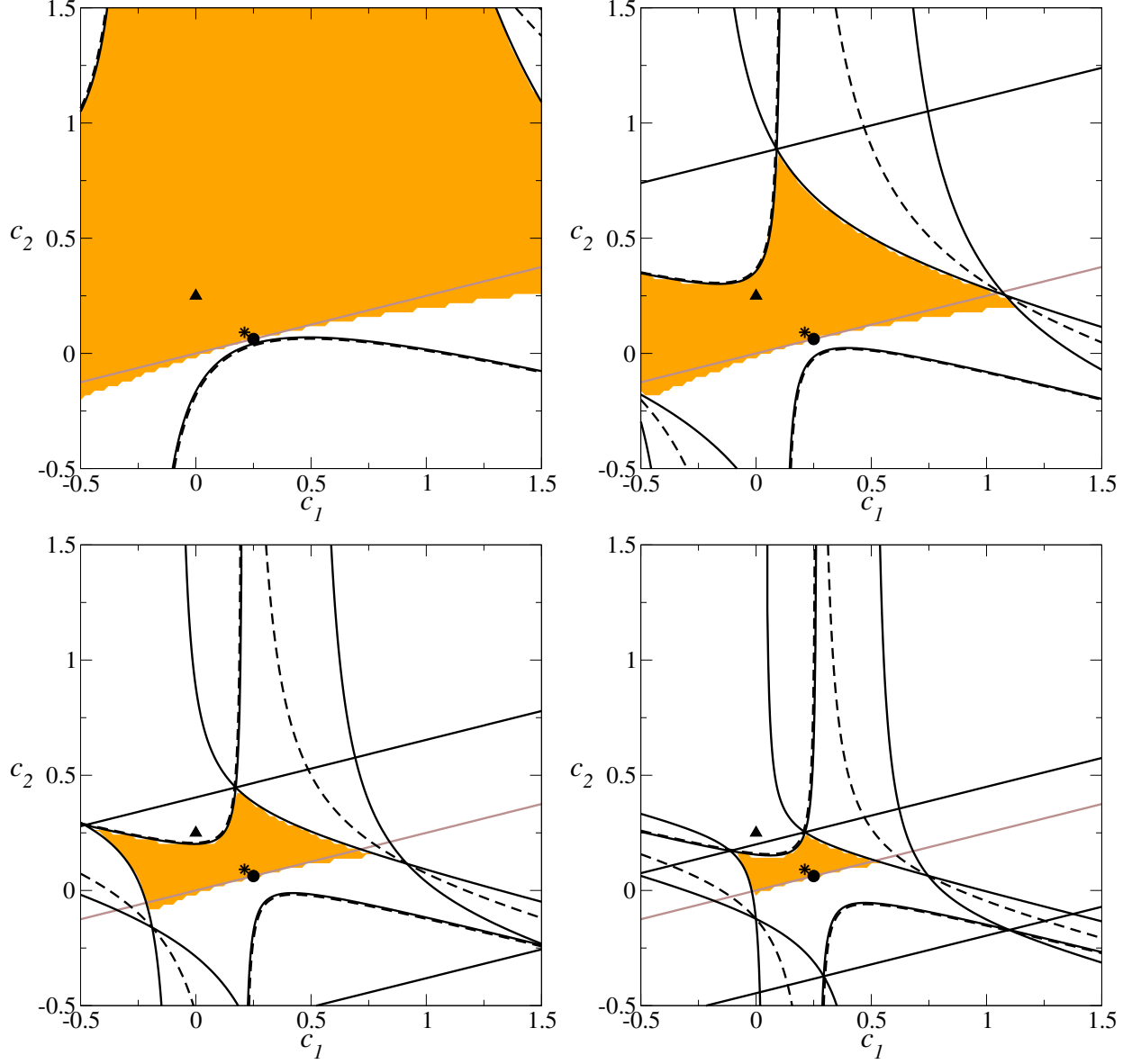


Figure 6: Dependence of the numerically determined stability region (orange area) on the (c_1, c_2) coefficients for the evolution of h using a third-order PIRK method. The boundaries (solid lines) of the stability region according to Eqs. (107)-(110) for $\bar{x} = 5.322$ (black lines) and $\bar{x} = 0$ (brown line), and the boundaries of the region $|\det(M_3)| \leq 1$, which partially coincide with the stability boundaries, are plotted. The values for the optimal third-order PIRK methods, $(c_1, c_2) = (1/4, 1/16)$ (PIRK3a, black circle) and $(c_1, c_2) = ((3 - \sqrt{3})/6, (-1 + \sqrt{3})/8)$ (PIRK3b, star symbol), and the third-order ERK scheme (black triangle), are also plotted.

performed a χ^2 minimization to determine the value of \bar{x} which fits better the boundaries of the stability region with the expressions (107)-(110). We obtain $\bar{x} = 5.322$ ($\chi^2 = 109.0$ for 255 degrees of freedom). For the numerical setup considered, we estimate $\bar{x}_{\min} = 6.945 \times 10^{-7} \ll 1$, so we consider as a boundary the condition (110) setting $x = 0$ (brown solid line in Fig. 6). The resulting boundaries (solid lines in Fig. 6) fit very well with the numerically estimated stability region (orange area in Fig. 6). The condition $|\det M_3| \leq 1$ (dashed lines in Fig 6) overestimate the stability region; however, the optimal values obtained in Sect. 4.5 (black circle and star symbol in Fig. 6) lay inside the stability region for all CFL factors studied. Since both values are very close, any of them could be used in the case of the wave equation for CFL factors close to unity. If we compare to the third-order IMEX-SSP3(4,3,3) scheme in [5], corresponding to $\mathcal{C}_1 = 0.24169426078821$ and $\mathcal{C}_2 = (1 - 3\mathcal{C}_1)/4 = 0.06872930440884$, the stability properties are very similar since the coefficients are very close to the optimal PIRK values, and therefore the method is numerically stable for the considered CFL factors.

The third-order ERK scheme corresponds to $(\mathcal{C}_1, \mathcal{C}_2) = (0, 1/4)$ (black triangle in Fig. 6). The eigenvalues of M_3 in this particular case are

$$e_{\pm} = 1 - \frac{x}{2} \pm \frac{1}{6} \sqrt{-x(x-6)^2}. \quad (113)$$

The condition $|e_{\pm}| \leq 1$ results in

$$0 \leq x \leq 3. \quad (114)$$

For the fitted value of \bar{x} , this condition restricts the stability of the third-order ERK scheme to $\text{CFL} < 0.751$. Accordingly, our numerical simulations show numerical stability for 0.5 and 0.7 CFL factors, but not for 0.8 and 0.9. We conclude that, although the third-order ERK scheme is stable, the time step is more restricted as in the third-order PIRK method.

6.2. Convergence

We have studied the convergence properties of the PIRK methods by performing series of 1D-spherically symmetric, 2D-axisymmetric and 3D simulations. In each one, we use reference models with resolutions $n_r = 50$, $(n_r, n_{\theta}) = (50, 16)$ and $(n_r, n_{\theta}, n_{\varphi}) = (50, 8, 32)$, respectively. We increase the resolutions in all directions by the following factors: 2, 4, 8, 16 and 32 (1D); 2, 4, 8 (2D); 1.5, 2, 4 (3D). The L_2 -norm of h after 1/4 period of oscillations, $t = \pi/\omega/2$, is used as an estimation of the error. To ensure that we measure the error due to the time discretization and not due to the spatial one, we choose the spatial order carefully. The time step in 1D, 2D and 3D simulations in spherical coordinates scales as $\Delta t_{1D} \sim \Delta r$, $\Delta t_{2D} \sim \Delta r \Delta \theta$, and $\Delta t_{3D} \sim \Delta r \Delta \theta \Delta \varphi$, respectively, i.e., if we increase the resolution in all directions by a factor 2, Δt decreases in a factor 2, 4 and 8, respectively. Therefore, to ensure that increasing resolution the spatial discretization errors decrease at least as fast as the time discretization errors, we choose fourth-order spatial discretization for the first-order methods, fourth (1D) and sixth-order (2D, 3D) for the second-order methods, fourth (1D), eighth (2D) and tenth-order (3D) for the third-order methods, and sixth (1D), tenth (2D) and twelfth-order (3D) for the fourth-order methods. In all cases, $\text{CFL} = 0.8$.

Fig. 7 shows the error as a function of the time step. Independently of the dimensionality of the simulation, the error falls with decreasing time step as expected from the convergence order of the method used (dashed lines). In the case of third-order methods, the numerically obtained order seems closer to 4 (dotted line); this is probably due to cancellations in the third-order time derivatives, for this particular test. Note that the error is limited by the machine accuracy (double precision was used) in the highest resolution simulations using the third and fourth-order methods, which produces an increase of the error with increasing resolution.

6.3. Cartesian coordinates

According to the stability analysis of Sect. 4, the results obtained for the wave equation should be independent of the coordinates used in the discretization of the PDEs. In order to test this, we have performed 1D, 2D and 3D numerical simulations of the scalar wave equation in Cartesian coordinates. Our

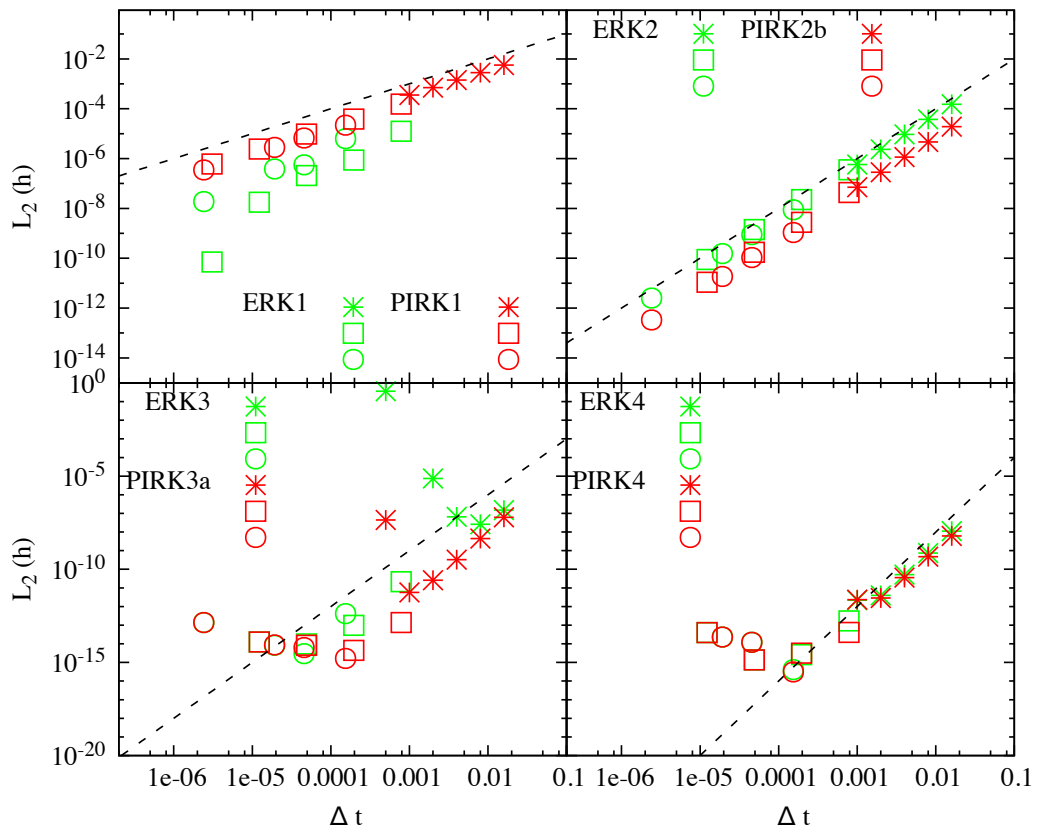


Figure 7: Numerical error estimation for series of 1D (stars), 2D (squares) and 3D (circles) simulations of a scalar wave in spherical coordinates, as a function of the time step, for first-order (upper left), second-order (upper right), third-order (lower left) and fourth-order (lower right) methods. Black-dashed lines corresponds to the expected order of convergence in each case.

computational domain is a box of size 1. We impose periodic boundary conditions. In this case, Eq. (83) has solutions of the form

$$h(x, y, z, t) \sim \sin(k_x x + \phi_x) \sin(k_y y + \phi_y) \sin(k_z z + \phi_z) \cos \omega t, \quad (115)$$

being k_x , k_y and k_z the wave number in the different directions, ϕ_x , ϕ_y and ϕ_z a phase, and $\omega = \sqrt{k_x^2 + k_y^2 + k_z^2}$ the oscillation frequency. The boundary conditions limit the possible choices of the wavenumbers to integer multiples of 2π . For our tests we have experimented with $k_i = 2\pi$ and $k_i = 4\pi$ ($i = x, y, z$). We have performed series of simulations comparing the PIRK methods with ERK methods at different resolutions (ranging from 100 points to 1000 points) and CFL numbers (ranging from 0.001 to 1).

For sake of brevity and to avoid repetition with the results in spherical coordinates, we will not describe in detail our numerical results using Cartesian coordinates. All the simulations that we have performed agree with the results in spherical coordinates in terms of stability properties of both PIRK and ERK methods, and in terms of convergence properties. Therefore, we can conclude that the performance of this methods is independent of the coordinates used in the spatial discretization as expected.

7. Application 3: non-linear wave equation

For our last test we consider the non-linear wave equation written as a first-order system in time,

$$\begin{aligned} \partial_t h &= A, \\ \partial_t A &= h_{xx} - V'(h), \end{aligned} \quad (116)$$

where $V(h)$ is a nonlinear function of h . Eqs. (116) form a system of Hamiltonian partial differential equations whose Hamiltonian is,

$$\mathcal{H} = \int \left(\frac{1}{2} A^2 + \frac{1}{2} h_x^2 + V(h) \right) dx. \quad (117)$$

Therefore, even if there are no general analytical solutions for this system, the Hamiltonian should be preserved during numerical evolutions and this can be used to test our numerical methods in the nonlinear regime. We use a nonlinear potential of the form $V(h) = h^4/4$. For this choice of $V(h)$, if the initial data are C^∞ , then the solution at any time will be C^∞ as well [34]. This system of equations is also known to develop odd-mode instabilities for sufficiently large amplitudes of h .

We have followed the test setup of [35] and solved equations in the domain $x \in [0, 2\pi]$ imposing periodic boundary conditions. Our initial data are $h_0(x) = a \cos(x) + 10^{-12} \sin(x)$ and $A_0(x) = 0$. The $\sin(x)$ term, used in [35], is used to excite in a controlled way the odd-mode instabilities. Those instabilities appear for values of $a > \sim 1.85$ [35]. We have performed numerical simulations with $a = 2$ using either 100 or 500 points and sixth-order discretization for the spatial derivatives, which is sufficient to properly resolve the dynamics of the system and to keep the spatial-discretization error below the time-discretization one. The linear part of Eq. (116) corresponds to a wave-equation with propagation speed 1. Therefore, a CFL condition for explicit methods can be computed and gives a maximum time-step of $\Delta t_{\max} = \Delta x$.

As a measure of the error in our numerical simulations we have used the time averaged L_2 -norm of the relative variation of the Hamiltonian during the simulation,

$$\text{error}(\mathcal{H}) = \sqrt{\frac{1}{t_{\text{end}}} \int_0^{t_{\text{end}}} \left(\frac{\mathcal{H}_0 - \mathcal{H}}{\mathcal{H}_0} \right)^2 dt}, \quad (118)$$

being $t_{\text{end}} = 2000$ (≈ 318 oscillation cycles) the end of the simulation, and \mathcal{H}_0 the initial value of the Hamiltonian. We consider a numerical evolution to be numerically unstable if this measure of the error exceeds 1. For those cases the error typically grows exponentially with time.

As an example for the typical evolution of a numerically stable simulation with 500 points and $\Delta t = 0.01 = 0.8\Delta t_{\max}$, the middle panel of Fig. 8 shows the time evolution of the Hamiltonian \mathcal{H} , which stays

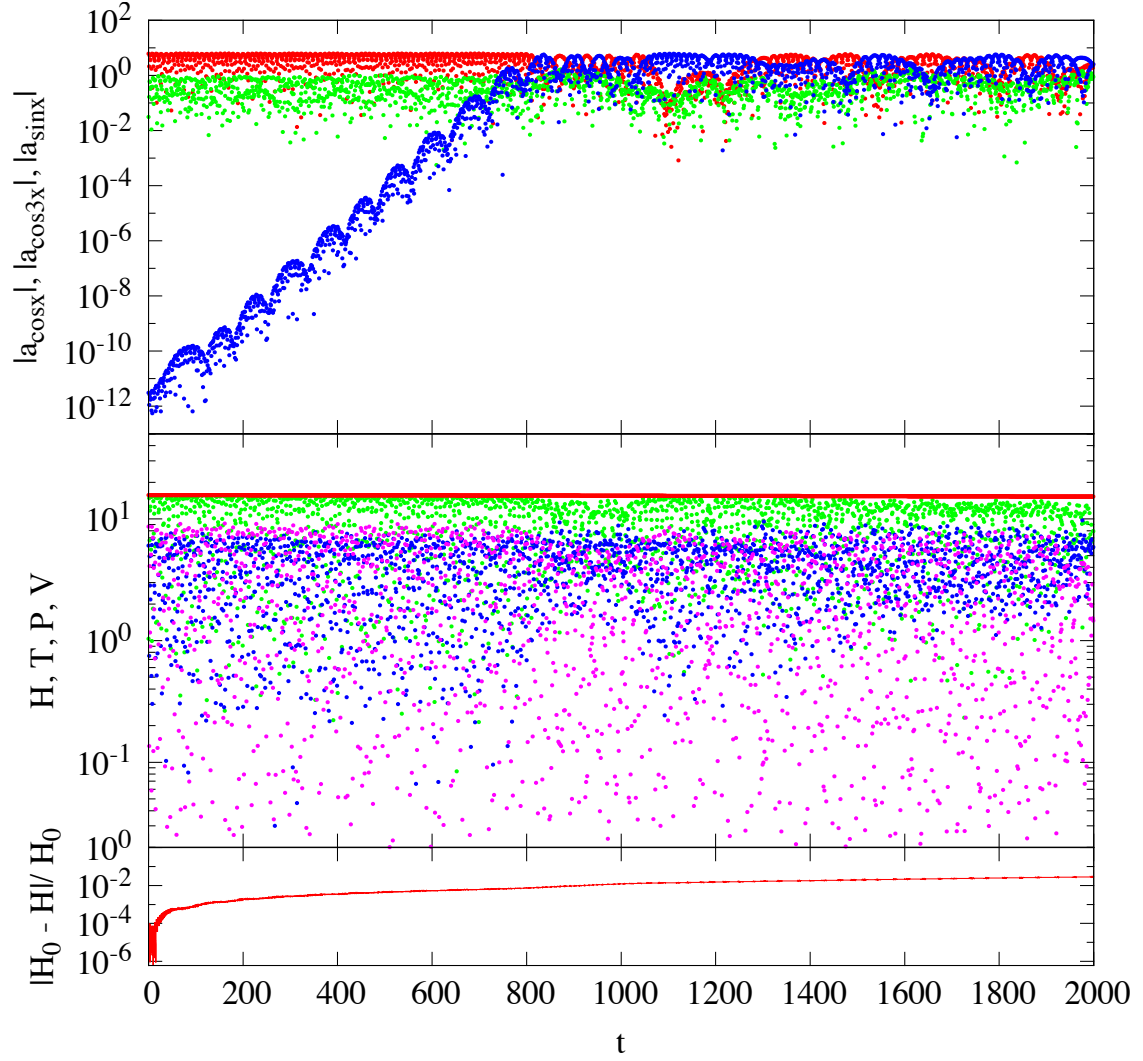


Figure 8: Time evolution of the nonlinear wave equation using the PIRK2a method, $\Delta t = 0.01$ and 500 points. Upper panel shows the overlap integrals for the original perturbation ($\cos x$, red points), the first overtone ($\cos 3x$, green points) and the odd-mode instability ($\sin x$, blue points). Middle panel shows the Hamiltonian, \mathcal{H} (red points), and the different contributions to the integral: \mathcal{T} (green points), \mathcal{P} (blue points) and \mathcal{V} (violet points). Lower panel shows the relative difference of \mathcal{H} and its initial value \mathcal{H}_0 .

Table 6: Maximum CFL in numerical simulations of the non-linear wave equation, for which no numerical instabilities developed, depending on the numerical method and the number of points used. In cases marked with "–" all numerical simulations developed numerical instabilities.

		number of points	
		100	500
method	ERK1	–	–
	PIRK1	0.8	0.8
	ERK2	–	–
	PIRK2a	0.8	0.8
	PIRK2b	0.9	0.9
	ERK3	0.7	0.7
	PIRK3a	1.0	1.0
	PIRK3b	1.0	1.0
	IMEX3	1.0	1.0
	ERK4	1.3	1.3
	PIRK4	1.8	1.8

constant within a few percent (lower panel). We also plot separately the different contributions to the Hamiltonian:

$$\mathcal{T} \equiv \int \frac{1}{2} A^2 dx, \quad (119)$$

$$\mathcal{P} \equiv \int \frac{1}{2} h_x^2 dx, \quad (120)$$

$$\mathcal{V} \equiv \int V(h) dx. \quad (121)$$

The contribution to the system of the nonlinear potential, \mathcal{V} , is non negligible and of the order of \mathcal{P} . Therefore, the evolution of the system is genuinely nonlinear. We have also computed the overlap integrals

$$a_{f(x)} \equiv \int h(x) f(x) dx, \quad (122)$$

using as trial functions the initial perturbation, $f(x) = \cos(x)$, an overtone $f(x) = \cos(3x)$ and an odd-mode, $f(x) = \sin(x)$, which is excited by the nonlinear interaction. The upper panel of Fig. 8 shows the time evolution of the time integrals, which are comparable to the results shown in [35].

Fig. 9 shows the convergence and stability of the PIRK methods in comparison with ERK methods. For this purpose we performed simulations with CFL factors ($\Delta t/\Delta t_{\max}$) ranging from 0.125 to 2. In almost all cases we were able to find a limiting CFL factor, within the range, above which numerical instabilities develop ($\text{error}(\mathcal{H}) \gg 1$); their values are shown in table 6. The exception are the first and second-order ERK methods for which all simulations developed numerical instabilities; this is consistent with the unconditionally unstable nature of those methods for wave-like equations, as seen in Sect. 4. In the third and fourth-order cases, the PIRK methods were stable for larger CFL numbers than ERK methods, by a factor ~ 1.4 . Note that the maximum CFL factor for both resolutions (100 and 500) is the same, but it corresponds to a different maximum time-step in each case.

The results in Fig. 9 show that for first and third-order methods the numerical error behaves as $\propto \Delta t$ and $\propto \Delta t^3$, respectively, as expected. For second and fourth-order methods the numerical error decays faster with decreasing Δt than expected, very close to $\propto \Delta t^3$ and $\propto \Delta t^5$, respectively. This behaviour is probably due to the particular symmetries of the problem at hand, which produce cancellations of even powers of Δt in the expansion of the error in terms of the time-step. In all cases the error achieved by the PIRK methods were smaller than that in the ERK methods by a factor $\sim 10 - 100$ and ~ 10 for the third and fourth-order cases, respectively. The behaviour of the IMEX-SSP3(4,3,3) (IMEX3 here) was similar to the PIRK methods in all cases regarding both the maximum CFL and the error.

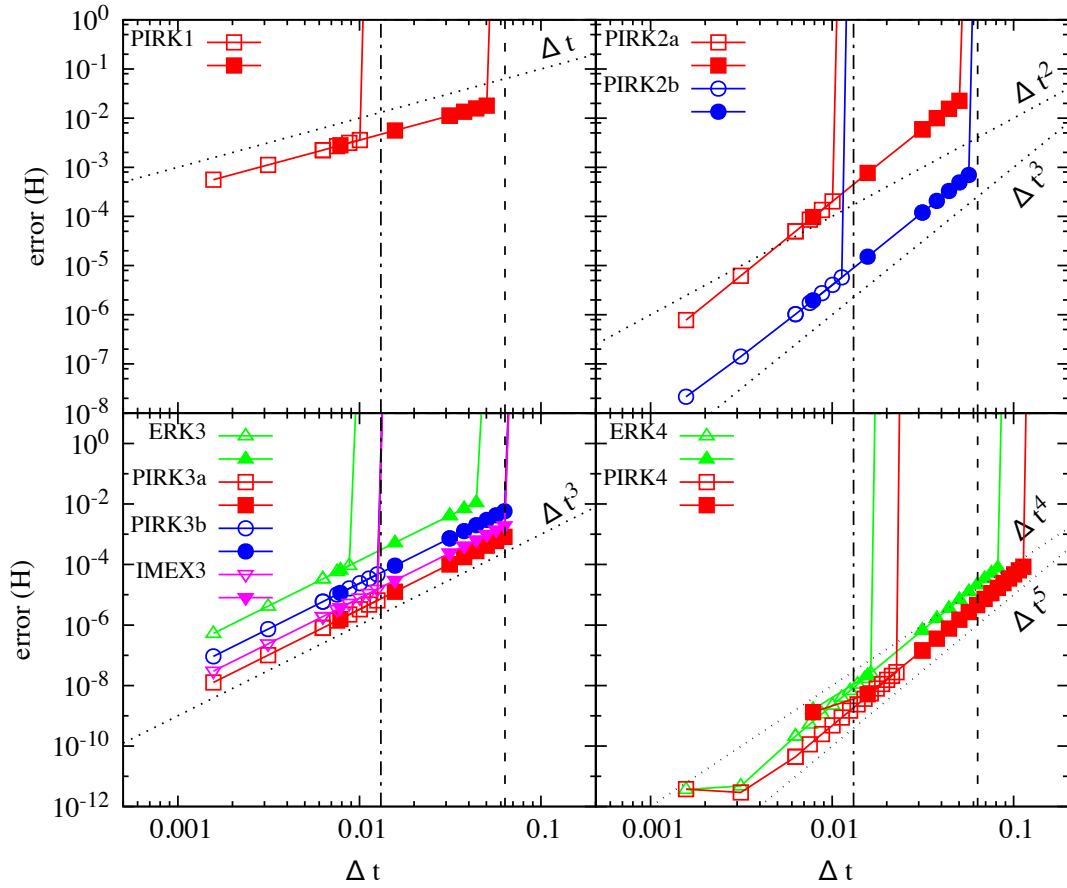


Figure 9: Time averaged L_2 -norm of the relative change of the Hamiltonian at the end of the simulation ($t = 2000$) in the evolution of the nonlinear wave equation, as a function of time-step Δt . Results for first (upper left panel), second (upper right), third (lower left) and fourth-order (lower right) methods are plotted for the case with 100 points (filled symbols) and 500 points (open symbols). Dotted lines show difference power dependence on Δt , for reference. Vertical lines show the CFL condition for the case with 100 (dashed lines) and 500 points (dot-dashed lines).

8. Conclusions

In this work we present a new class of Runge-Kutta methods, the PIRK schemes, tailored to solve wave-like systems of non-linear PDEs. Methods up to fourth-order of convergence have been derived. The new methods are partially implicit in the sense that a proper subset of the equations of the system contains some terms which are treated implicitly. Optimal SSP ERK methods are recovered when implicitly treated parts are neglected. Although the implicit parts confer stability to the system, no analytical or numerical inversion of any operator is required, and the computational costs of the derived PIRK methods are comparable to those of the ERK ones.

To derive the new methods we first relate the coefficients of a s -stages PIRK method to a $s + 1$ -stages IMEX one, and then we impose the order conditions to find the relations between the different coefficients of the method. The remaining free coefficients in each case are chosen according to stability criteria. For this purpose we analyse the determinant of the matrix which updates values from one time-step to the next one. Although this condition is less restrictive than the corresponding bound on the eigenvalues, which is the definition of the linear stability, we show, according to the numerical simulations performed, that the coefficients lead to numerically stable integrations.

We have successfully applied the derived PIRK methods to several cases: the evolution of a system of ODEs, the evolution of a scalar wave-equation and the evolution of a non-linear scalar wave-equation. We have studied the numerical stability of the systems and checked the convergence order of the PIRK methods in all the simulations, which were in agreement with the expected ones.

In the case of the scalar wave-equation, for first, second and third-order methods, we have studied the numerical stability of the system depending on the free coefficients of the method and the CFL factor. This kind of analysis was numerically not feasible for the fourth-order PIRK method because of its high computational cost of having to explore the 5-dimensional space of free parameters. We have been able to compare the stability region estimated numerically with that obtained from the eigenvalues of the system, with excellent agreement. In all cases our optimal choice for the coefficients lays within the stability region, which shrinks with increasing resolution. This result is interesting because, despite of the fact that we computed the coefficients using the less restrictive condition for the determinant, the result still seems to be optimal. We think this is encouraging, as this kind of analysis could be used to compute optimal schemes for higher-order methods to evolve in time wave-like equations, without the complexity of having to work with the eigenvalues.

Applied to wave-like equations, stable numerical evolutions with the PIRK methods were possible using time-steps larger than in the traditional ERK methods. Stability properties for first and second-order methods are also superior to the ERK methods, the latter ones resulting to be unconditionally unstable in both the linear stability analysis and the numerical simulations. The third and fourth-order ERK methods are stable, but with a lower maximum time-step achievable than in the corresponding third and fourth-order PIRK methods. We suspect that the success of ERK methods in other works applied to wave-like equations could be due to the wide spread use of numerical-dissipation terms (e.g. [23]), which could avoid the growth of small-scale unstable modes, as well as a sufficient small time-step in order to control the growth of the numerical errors. The PIRK methods do not need any numerical-dissipation term to get stable evolutions nor suffer from such time-step restrictions. Compared to IMEX methods, the presented second and third-order PIRK methods showed similar stability and convergence properties. However, some work had to be done to adapt the IMEX-SSP2(2,2,2) and the IMEX-SSP3(4,3,3) of [5] to eliminate unnecessary stages.

To quantify the advantage of the PIRK methods over the ERK ones, we can estimate the computational cost of each numerical simulation presented in Sects. 5, 6 and 7 computing the number of evaluations of the L_i operators per unit time, which is proportional to $s/\Delta t$, s being the number of stages of the method. Since the bulk of the computational cost of most numerical applications comes from the evaluation of the L_i sources, this is a good estimator of the computational cost in real applications. In Fig. 10 we plot the computational cost as a function of the numerical error measured in the simulation, for the different numerical methods and tests presented in this work. For a given accuracy goal, the plots tell us which is the numerical method with less computational cost. We have omitted in the plot those cases in which the error was decaying fastest than the expected order of convergence; in those cases the error is particularly

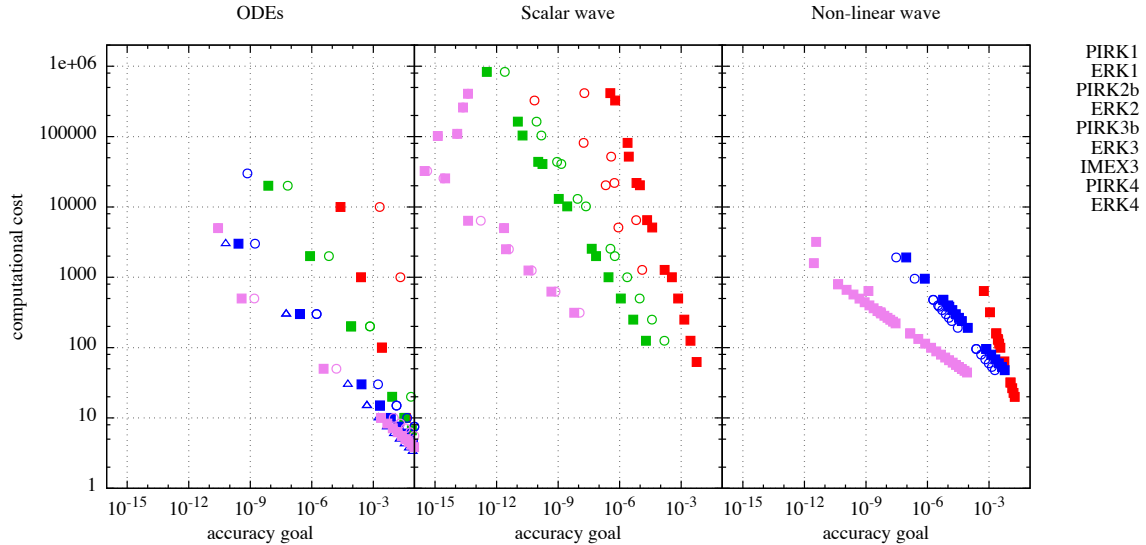


Figure 10: Computational cost, measured as the number of evaluations of the L_i operators per unit time, as a function of the error in the solution for the three tests presented in this work and different numerical methods.

low due to symmetries of the particular test under consideration and cannot be used to estimate the error in a general situation. In general, higher-order methods are less costly to obtain the same numerical error. Comparing different methods, the PIRK schemes are less costly than the ERK ones of the same order. The IMEX schemes behave similarly to the PIRK methods of the same order. Taking into account of all the methods tested, the PIRK4 scheme is the most efficient one in terms of computational cost.

An straightforward application of the PIRK methods is the numerical integration of Einstein equations, which involves the solution of a hyperbolic system of non-linear equations with a wave-like structure. This system of equations is of great interest for the numerical relativity community, in order to generate gravitational wave templates for the upcoming gravitational wave detectors (LIGO, VIRGO and KAGRA). As a matter of fact, the PIRK methods presented in the present work have already been applied to evolve Einstein equations [36, 37, 38, 39, 40, 41, 42, 44, 43, 45, 46, 47]. These recent works represent the first multidimensional simulations of Einstein equations in spherical coordinates, that traditionally have been performed in Cartesian coordinates, and the use of the PIRK methods was critical for the success of such simulations.

Appendix A. Stability conditions for second-order PIRK methods

In this appendix we detail the derivation of the inequalities (37) and (38). We would like to guarantee

$$-4 \leq K_1 + \lambda\alpha_2 K_2(1 - 2C_1 + 2C_2) + \lambda^2\alpha_2^2(2C_2 - C_1 - 2C_1C_2) \leq 4, \quad (\text{A.1})$$

for $\omega_i = 0, \pm 1$, $i = 1, 2$, and in the cases $|\lambda\alpha_2| \gg 1$, $\lambda\alpha_2 \approx -1$ and $|\lambda\alpha_2| \ll 1$:

1. Upper bound, $\omega_1 = \omega_2 = \pm 1$: $K_1 = 4$, $K_2 = 0$. In all the cases we require $2C_2(1 - C_1) - C_1 \leq 0$.
2. Upper bound, $\omega_1 = -\omega_2 = -\pm 1$: $K_1 = 4$, $K_2 = 2$.

For $|\lambda\alpha_2| \ll 1$, we require $0 \leq 1 - 2C_1 + 2C_2$. This condition is sufficient for the cases $|\lambda\alpha_2| \gg 1$ and $\lambda\alpha_2 \approx -1$.

3. Upper bound, $\omega_1 = \omega_2 = 0$: $K_1 = 1, K_2 = 1$. Previous derived conditions are sufficient for all the cases.
4. Lower bound, $\omega_1 = \omega_2 = \pm 1$: $K_1 = 4, K_2 = 0$. In all the cases we require $-8 \leq \lambda^2 \alpha_2^2 (2\mathcal{C}_2 - \mathcal{C}_1 - 2\mathcal{C}_1\mathcal{C}_2)$. This condition will be satisfied by the following ones.
5. Lower bound, $\omega_1 = -\omega_2 = -\pm 1$: $K_1 = 4, K_2 = 2$.
 - For $|\lambda\alpha_2| \ll 1$, we require $-4 \leq \lambda\alpha_2(1 - 2\mathcal{C}_1 + 2\mathcal{C}_2)$.
 - For $|\lambda\alpha_2| \gg 1$, previous derived conditions are sufficient.
 - For $\lambda\alpha_2 \approx -1$, we require $0 \leq 6 + 5\mathcal{C}_1 - 6\mathcal{C}_2 + 2\mathcal{C}_1\mathcal{C}_2$.
6. Lower bound, $\omega_1 = \omega_2 = 0$: $K_1 = 1, K_2 = 1$.
 - For $|\lambda\alpha_2| \ll 1$, previous derived conditions are sufficient.
 - For $|\lambda\alpha_2| \gg 1$, we require $-5 \leq \lambda^2 \alpha_2^2 (2\mathcal{C}_2 - \mathcal{C}_1 - 2\mathcal{C}_1\mathcal{C}_2)$.
 - For $\lambda\alpha_2 \approx -1$, we require $0 \leq 4 + \mathcal{C}_1 - 2\mathcal{C}_1\mathcal{C}_2$.

Appendix B. Stability conditions for third-order PIRK methods

In this appendix we detail the derivation of the inequalities (54) and (55). We would like to guarantee

$$\begin{aligned}
 -1 \leq & \frac{K_1}{36} + \frac{\lambda\alpha_2 K_2 (-1 + \mathcal{C}_1 - 4\mathcal{C}_2)}{24} \\
 & + \frac{\lambda^2 \alpha_2^2}{12} [\mathcal{C}_1 - 4\mathcal{C}_2 + (\text{dex} - 1)(4\mathcal{C}_2 - \mathcal{C}_1^2 - 4\mathcal{C}_1\mathcal{C}_2)] \\
 & - \frac{\lambda^3 \alpha_2^3}{72} [-1 + 3(1 - 2\mathcal{C}_1)(\mathcal{C}_1 + 4\mathcal{C}_2)] \leq 1.
 \end{aligned} \tag{B.1}$$

for $\omega_i = \pm 1, i = 1, 2$, and in the cases $|\lambda\alpha_2| \gg 1, \lambda\alpha_2 \approx -1$ and $|\lambda\alpha_2| \ll 1$:

1. Upper bound, $\omega_1 = \omega_2 = 1$: $K_1 = 36, K_2 = 0, \text{dex} = 1$.
 - For $|\lambda\alpha_2| \ll 1$, we require $\mathcal{C}_1 - 4\mathcal{C}_2 \leq 0$.
 - For $|\lambda\alpha_2| \gg 1$, we require $-1 + 3(1 - 2\mathcal{C}_1)(\mathcal{C}_1 + 4\mathcal{C}_2) \leq 0$.
 - For $\lambda\alpha_2 \approx -1$, previous derived conditions in this appendix are sufficient.
2. Upper bound, $\omega_1 = \omega_2 = -1$: $K_1 = 4, K_2 = 8, \text{dex} = 1$.
 - For $|\lambda\alpha_2| \ll 1$, we require $\lambda\alpha_2(-1 + \mathcal{C}_1 - 4\mathcal{C}_2) \leq 8/3$.
 - For $|\lambda\alpha_2| \gg 1$, previous derived conditions are sufficient.
 - For $\lambda\alpha_2 \approx -1$, we require $0 \leq 41 + 18(\mathcal{C}_1 - 4\mathcal{C}_2) - 3(1 - 2\mathcal{C}_1)(\mathcal{C}_1 + 4\mathcal{C}_2)$. Taking into account previous derived conditions, it is sufficient to require $-20/9 \leq \mathcal{C}_1 - 4\mathcal{C}_2$.
3. Upper bound, $\omega_1 = 1 = -\omega_2$ or $\omega_2 = 1 = -\omega_1$: $K_1 = -12, K_2 = 8, \text{dex} = -1$.
 - For $|\lambda\alpha_2| \ll 1$, previous derived conditions are sufficient.
 - For $|\lambda\alpha_2| \gg 1$, previous derived conditions are sufficient.
 - For $\lambda\alpha_2 \approx -1$, we require $0 \leq 73 + 18\mathcal{C}_1^2 - 180\mathcal{C}_2 + 9\mathcal{C}_1(3 + 8\mathcal{C}_2)$.
4. Lower bound, $\omega_1 = \omega_2 = 1$: $K_1 = 36, K_2 = 0, \text{dex} = 1$.
 - For $|\lambda\alpha_2| \ll 1$, we require $-24 \leq \lambda^2 \alpha_2^2 (\mathcal{C}_1 - 4\mathcal{C}_2)$.
 - For $|\lambda\alpha_2| \gg 1$, we require $\lambda^3 \alpha_2^3 [-1 + 3(1 - 2\mathcal{C}_1)(\mathcal{C}_1 + 4\mathcal{C}_2)] \leq 144$. This condition will be satisfied by following ones.
 - For $\lambda\alpha_2 \approx -1$, we require $0 \leq 9\mathcal{C}_1 - 12\mathcal{C}_2 - 6\mathcal{C}_1^2 - 24\mathcal{C}_1\mathcal{C}_2 + 143$.

5. Lower bound, $\omega_1 = \omega_2 = -1$: $K_1 = 4$, $K_2 = 8$, $\text{dex} = 1$.

For $|\lambda\alpha_2| \ll 1$, previous derived conditions are sufficient.

For $|\lambda\alpha_2| \gg 1$, we require $\lambda^3\alpha_2^3[-1 + 3(1 - 2\mathcal{C}_1)(\mathcal{C}_1 + 4\mathcal{C}_2)] \leq 80$. This condition will be satisfied by following ones.

For $\lambda\alpha_2 \approx -1$, we require $0 \leq 103 - 15\mathcal{C}_1 - 6\mathcal{C}_1^2 + 84\mathcal{C}_2 - 24\mathcal{C}_1\mathcal{C}_2$.

6. Lower bound, $\omega_1 = 1 = -\omega_2$ or $\omega_2 = 1 = -\omega_1$: $K_1 = -12$, $K_2 = 8$, $\text{dex} = -1$.

For $|\lambda\alpha_2| \ll 1$, previous derived conditions are sufficient.

For $|\lambda\alpha_2| \gg 1$, we require $\lambda^3\alpha_2^3[-1 + 3(1 - 2\mathcal{C}_1)(\mathcal{C}_1 + 4\mathcal{C}_2)] \leq 48$.

For $\lambda\alpha_2 \approx -1$, we require $0 \leq 6\mathcal{C}_1^2 - 15\mathcal{C}_1 + 36\mathcal{C}_2 + 24\mathcal{C}_1\mathcal{C}_2 + 71$.

Acknowledgements

This work was supported by the European Research Council (Starting Independent Research Grant CAMAP-259276), the Spanish Ministerio de Economía y Competitividad (grants AYA2013-40979-P and AYA2015-66899-C2-1-P) and the Generalitat Valenciana (PROMETEO-II-2014-069).

References

- [1] Butcher, J.C.: Numerical Methods for Ordinary Differential Equations, 2nd ed. J. Wiley, Chichester (2008)
- [2] Asher, U.M., Ruuth, S.J., Wetton, B.T.R.: Implicit-explicit methods for time-dependent PDE's. SIAM J. Num. Anal. 32, 797 (1995)
- [3] Asher, U.M., Ruuth, S.J., Spiteri, R.J.: Implicit-explicit Runge-Kutta methods for time-dependent partial differential equations. Appl. Num. Math. 25, 151 (1997)
- [4] Pareschi, L.: Central differencing based numerical schemes for hyperbolic conservation laws with relaxation terms. SIAM J. Num. Anal. 39, 1395 (2001)
- [5] Pareschi, L., Russo, G.: Implicit-explicit Runge-Kutta methods and application to hyperbolic systems with relaxation. J. Sci. Comput. 25, 129 (2005)
- [6] de Vogelaere, R.: Methods of integration which preserve the contact transformation property of the Hamiltonian equations, Report No. 4, Dept. Math., Univ. of Notre Dame (1956)
- [7] Hairer, E., Wanner, G., Lubich, C.: Geometric numerical integration: Structure-preserving algorithms for ordinary differential equations, 2nd ed. Springer-verlag, Berlin (2002)
- [8] Hairer, E., Wanner: Solving ordinary differential equations II. Stiff and differential-algebraic problems, 2nd ed. Springer-verlag, Berlin (2002)
- [9] Söderlind, G., Jay, L., Calvo, M.: Stiffness 1952:2012: Sixty years in search of a definition. BIT Numer. Math. 55, 531-558 (2015)
- [10] Curtiss, C.F. & Hirschfelder, J.O.: Integration of stiff equations. PNAS, 38, 235-243 (1952)
- [11] Vlach, J. and Singhal, K.: Computer methods for circuit analysis and design.
- [12] Rapaport, D.C.: The art of molecular dynamics simulations, 2nd ed. Cambridge University Press, Cambridge, UK (2004)
- [13] Yee, K: "Numerical solution of initial boundary value problems involving Maxwell's equations in isotropic media". IEEE Transactions on Antennas and Propagation 14 (3): 302-307 (1966)
- [14] Baraff, D., Witkin, A.: Large steps in cloth simulation, in SIGGRAPH, ACM, pp 43-54 (1998)
- [15] Asher, U. M.: Numerical methods for evolutionary differential equations. SIAM, Philadelphia, USA (2008).
- [16] Niiranen J.: Fast and accurate symmetric Euler algorithm for electromechanical simulations. in Electrimacs proceedings vol. 1, pp 71-78 (1999)
- [17] Fang, H., Lin, G., Zhang, R: The first-order symplectic Euler method for simulation of GPR wave propagation in pavement structure IEEE Transactions on geoscience and remote sensing, vol. 51. no 1, 93-98 (2013)
- [18] Holland, R: Implicit three-dimensional finite differencing of Maxwell's equations. IEEE Trans. Nucl. Sci., vol. NS-31, pp. 1322-1326 (1984)
- [19] Moxley III, F.L., Byrnes, T., Fujiwara, F., Weizhong, D.: A generalized finite-difference time-domain scheme for solving nonlinear Schrödinger equations. Comp. Phys. Comm. 183, 2434-2440 (2012)
- [20] Pretorius, F.: Numerical relativity using a generalized harmonic decomposition. Class. Quant. Grav. 22, 425-451 (2005)
- [21] Baker, J. G., Centrella, D.C., Koppitz, M, van Meter, J.: Gravitational-Wave Extraction from an Inspiral Configuration of Merging Black Holes. Phys. Rev. Lett., 96, 111102 (2006)
- [22] Centrella, J., Baker, J. G., Kelly, B. J., van Meter, J. R.: Black-hole binaries, gravitational waves, and numerical relativity. Rev. Mod. Phys. 82, 3069 (2010)
- [23] Kreiss, H.-O., Olinger, J.: Methods for the Approximate Solution of Time Dependent Problems. World Meteorological Organization, New York (1973)

- [24] Gottlieb, S., Shu, C.-W.: Total Variation Diminishing Runge-Kutta schemes. *Math. Compt.* 67, 73–85 (1998)
- [25] Gottlieb, S., Shu, C.-W., Tadmor, E.: Strong-stability-preserving high order time discretization methods. *SIAM Review* 43, 89–112 (2001)
- [26] Shu, C.-W., Osher, S.: Efficient implementation of essentially non-oscillatory shock-capturing schemes. *J. Comput. Phys.* 77, 439 (1988)
- [27] Kraaijevanger, J.F.B.M.: Contractivity of Runge-Kutta methods. *BIT* 31, 482–528 (1991)
- [28] Spiteri, R.J., Ruuth, S.J.: A new class of optimal high-order strong-stability-preserving time discretization methods. *SIAM J. Numer. Anal.* 40, 469–491 (2002)
- [29] Ruuth, S.J.: Global optimization of explicit strong-stability-preserving Runge-Kutta methods. *Math. Comput.* 75, 183–207 (2006)
- [30] Ruuth, S.J., Spiteri, R.J.: High-order strong-stability-preserving Runge-Kutta methods with downwind-biased spatial discretizations. *SIAM J. Numer. Anal.* 42, 974 (2004)
- [31] Kennedy, C.A., Carpenter, M.H.: Additive Runge-Kutta schemes for convection-diffusion-reaction equations. *Appl. Numer. Math.* 44, 139–181 (2003)
- [32] Hundsdorfer, W., Verwer, J.G.: *Numerical Solution of Time-Dependent Advection-Diffusion-Reaction Equations*. Springer-Verlag, Berlin (2003)
- [33] *Handbook of Mathematical Functions with Formulas, Graphs, and Mathematical Tables*. Abramowitz, M., Stegun, I.A. (eds.), pp. 878–879, and 883. Dover, New York (1972)
- [34] Strauss, W.A.: *Nonlinear wave equations*. AMS Regional Conference Series no. 73. AMS, Providence (1989)
- [35] MacLachlan, R.: Symplectic integration of Hamiltonian wave equations. *Numer. Math.*, 66, 465–492 (1994)
- [36] Cordero-Carrión, I., Cerdá-Durán, P., Ibáñez, J.M.: Gravitational waves in dynamical spacetimes with matter content in the Fully Constrained Formulation. *Phys. Rev. D* 85, 044023 (2012)
- [37] Montero, P., Cordero-Carrión, I.: BSSN equations in spherical coordinates without regularization: Vacuum and nonvacuum spherically symmetric spacetimes. *Phys. Rev. D* 85, 124037 (2012)
- [38] Baumgarte, T.W., Montero, P., Cordero-Carrión, I., Müller, E.: Numerical relativity in spherical polar coordinates: Evolution calculations with the BSSN formulation. *Phys. Rev. D* 87, 044026 (2013)
- [39] Hilditch, D., Baumgarte, T.W., Weyhausen, A., Dietrich, T., Bruegmann, B., Montero, P., Müller, E.: Collapse of Nonlinear Gravitational Waves in Moving-Puncture Coordinates. *Phys. Rev. D* 88, 103009 (2013)
- [40] Sanchis-Gual, N., Montero, P., Font, J.A., Müller, E., Baumgarte, T.W.: Fully covariant and conformal formulation of the Z4 system in a reference-metric approach: comparison with the BSSN formulation in spherical symmetry. *Phys. Rev. D* 89, 104033 (2014)
- [41] Requier, J., Cordero-Carrión, I., Füzfa, A.: Fully relativistic nonlinear cosmological evolution in spherical symmetry using the BSSN formalism. *Phys. Rev. D* 91, 024025 (2015)
- [42] Sanchis-Gual, N., Degollado, J.C., Montero, P., Font, J.A.: Quasi-stationary solutions of self-gravitating scalar fields around black holes. *Phys. Rev. D* 91, 043005 (2015)
- [43] Baumgarte, T.W., Montero, P., Müller, E.: *Numerical Relativity in Spherical Polar Coordinates: Off-center Simulations*. *Phys. Rev. D* 91, 064035 (2015)
- [44] Sanchis-Gual, N., Degollado, J.C., Montero, P., Font, J.A., Mewes, V.: Quasistationary solutions of self-gravitating scalar fields around collapsing stars. *Phys. Rev. D* 92, 083001 (2015)
- [45] Requier, J., Füzfa, A., Cordero-Carrión, I.: Nonlinear cosmological spherical collapse of quintessence. *Phys. Rev. D* 93, 043533 (2016)
- [46] Sanchis-Gual, N., Degollado, J.C., Herdeiro, C., Font, J.A., Montero, P.: Dynamical formation of a Reissner-Nordström black hole with scalar hair in a cavity. *Phys. Rev. D* 94, 044061 (2016)
- [47] Sanchis-Gual, N., Degollado, J.C., Izquierdo, P., Font, J.A., Montero, P.: Quasistationary solutions of scalar fields around accreting black holes. *Phys. Rev. D* 94, 043004 (2016)